AGU PUBLICATIONS

Tectonics

RESEARCH ARTICLE
10.1002/2014TC003522

Key Points:
- Paleocene rocks bracket India-Asia collision at 60 to 58.5 Ma
- Gangetic foreland basin migrated 1300 km across India
- Implications for single-stage and two-stage collisions are discussed

Supporting Information:
- Readme
- Table S1

Correspondence to:
P. G. DeCelles,
decelles@email.Arizona.EDU

Citation:
DeCelles, P. G., P. Kapp, G. E. Gehrels, and L. Ding (2014), Paleocene-Eocene foreland basin evolution in the Himalaya of southern Tibet and Nepal: Implications for the age of initial India-Asia collision, *Tectonics*, *33*, doi:10.1002/2014TC003522.

Received 4 JAN 2014
Accepted 7 MAY 2014
Accepted article online 12 MAY 2014

Paleocene-Eocene foreland basin evolution in the Himalaya of southern Tibet and Nepal: Implications for the age of initial India-Asia collision

P. G. DeCelles[1], P. Kapp[1], G. E. Gehrels[1], and L. Ding[2]

[1]Department of Geosciences, University of Arizona, Tucson, Arizona, USA, [2]Key Laboratory of Continental Collision and Plateau Uplift, Institute of Tibetan Plateau Research, Chinese Academy of Sciences, Beijing, China

Abstract Siliciclastic sedimentary rocks derived from the southern Lhasa terrane, sitting depositionally upon rocks of the northern Indian passive continental margin, provide an estimate of the age of initial contact between the continental parts of the Indian and Asian plates. We report sedimentological, sedimentary petrological, and geochronological data from Upper Cretaceous-Paleocene strata in the Sangdanlin section, located along the southern flank of the Indus-Yarlung suture zone in southern Tibet. This is probably the most proximal, and therefore the oldest, record of the India-Asia collision. These strata were deposited by high-density turbidity currents (or concentrated density flows) and suspension settling of pelagic biogenic debris in a deep-marine setting. An abrupt change from quartz-arenitic to feldspatholithic sandstone compositions marks the transition from Indian to Asian sediment provenance. The abrupt compositional change is accompanied by changes in U-Pb ages of detrital zircons diagnostic of a sediment provenance reversal, from Indian to Asian sources. The timing of the transition is bracketed between ~60 Ma and 58.5 ± 0.6 Ma by detrital zircon U-Pb ages and zircon U-Pb ages from a tuffaceous bed in the upper part of the section. In the context of a palinspastically restored regional paleogeographic framework, data from the Sangdanlin section combined with previously published data from the northern Tethyan Himalaya and the frontal Nepalese Lesser Himalaya and Subhimalaya suggest that a flexural wave migrated ~1300 km southward across what is now the Himalayan thrust belt from Paleocene time to the present.

1. Introduction

Much effort has been expended to determine the timing of intercontinental collision between India and southern Asia [e.g., *Garzanti et al.*, 1987; *Searle et al.*, 1987; *Dewey et al.*, 1988; *Rowley*, 1996; *Yin and Harrison*, 2000; *Guillot et al.*, 2003; *Ding et al.*, 2005; *Leech et al.*, 2005; *Green et al.*, 2008; *Najman et al.*, 2010; *Cai et al.*, 2011; *Clift et al.*, 2013]; this stems partly from the fact that so many important geological, climatological, oceanographical, geophysical, geochemical, and paleobiological phenomena seem to have been stimulated by the ongoing collision [e.g., *Jaeger et al.*, 1989; *Métivier et al.*, 1999; *Quade et al.*, 2003; *Ravizza and Zachos*, 2003; *Bickle et al.*, 2005; *Singh et al.*, 2005; *Clift*, 2006; *Yin*, 2006; *Hren et al.*, 2007; *Dupont-Nivet et al.*, 2008; *Molnar et al.*, 2010]. Several criteria have been proposed for defining the onset of the India-Asia collision [e.g., *Rowley*, 1996; *Guillot et al.*, 2003; *Leech et al.*, 2005; *Green et al.*, 2008]. In principle, the onset of intercontinental collision is defined as the time at which the two continents come into physical contact. Continents scatter about themselves halos of erosional detritus that reflect their own peculiar lithological compositions. As two continents approach during an impending collision, their respective detrital aprons will comingle. Although turbidite fans constructed of continental detritus may extend much more than 1000 km offshore, they generally are deposited upon oceanic crust at abyssal depths. Thus, when the detritus of one continental landmass is deposited upon the continental shelf or slope of another continental landmass, the two opposing continents are engaged in initial collision. The inherent topographic and bathymetric asymmetry of the impending collisional landscape, with a subduction zone and relatively high elevation magmatic arc along the margin of the upper plate and a marine passive margin along the leading edge of the lower plate, places the detrital record of initial approach and collision onto the lower plate.

Based on this simple principle, much work on the India-Asia collision problem has focused on dating siliciclastic sedimentary rocks that contain detritus derived from Asia and deposited upon the northern

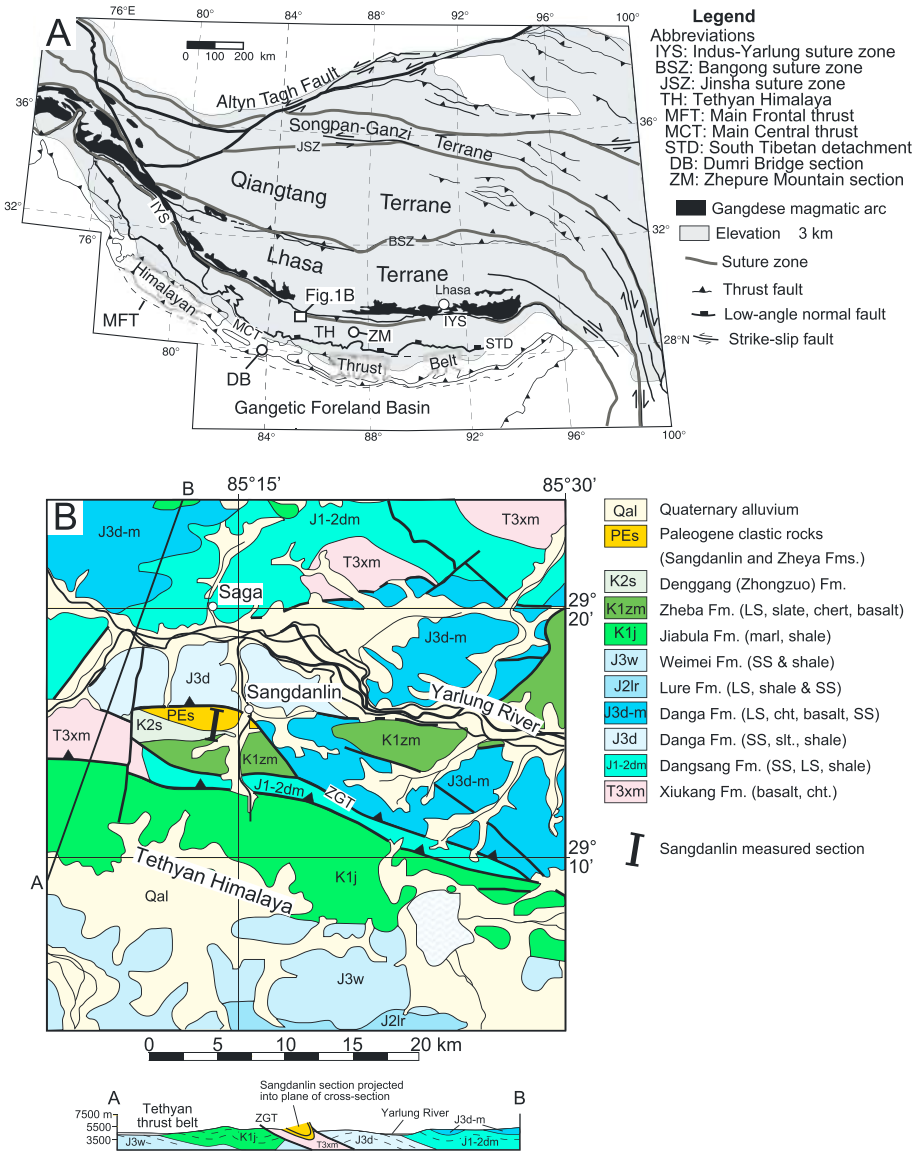

Figure 1. (a) Tectonic sketch map of the Tibetan Plateau, highlighting region of elevation >3 km and tectonic features of the Indus-Yarlung suture zone and Himalayan thrust belt [after *Yin and Harrison*, 2000]. (b) Geological map and cross section of the Sangdanlin study area, after *Yang et al.* [2003], *Ding et al.* [2005], and our own field observations.

outboard flank of Indian continental lithosphere as it entered the oceanic trench that marked the southern flank of the Asian landmass [e.g., *Garzanti et al.*, 1987; *Rowley*, 1996, 1998; *Wang et al.*, 2002; *Ding et al.*, 2005; *Zhu et al.*, 2005; *Najman*, 2006; *Aitchison et al.*, 2007; *Green et al.*, 2008; *Najman et al.*, 2008, 2010; *Henderson et al.*, 2010; *Wang et al.*, 2011; *Cai et al.*, 2011; *Hu et al.*, 2012; *Zhang et al.*, 2012; *Clift et al.*, 2013]. These Upper Cretaceous through lower Eocene rocks now crop out directly south of the belt of tectonic and sedimentary mélanges that mark the Indus-Yarlung suture (IYS) zone between India and Asia, and in the northern, or Tethyan, portion of the Himalayan thrust belt. Often ignored in considerations of the timing of initial collision are Eocene rocks that contain a record of the early collision cropping out within the Lesser Himalayan and Subhimalayan zones along the southern flank of the Himalayan thrust belt (Figure 1a) [*Sakai*, 1983; *Najman et al.*, 1993; *Critelli and Garzanti*, 1994; *Pivnik and Wells*, 1996; *Burbank et al.*, 1996; *DeCelles et al.*, 1998a, 2004; *Najman and Garzanti*, 2000; *Najman et al.*, 2005; *Jain et al.*, 2009; *Ravikant et al.*, 2011]. No attempt has been made to link the Paleogene records from the northern Himalaya and IYS zone with those from the southern part of the Himalaya within a synoptic, palinspastic framework.

In this paper we provide geochronological and sedimentary provenance data from upper Paleocene-lower Eocene strata in the IYS zone in the Sangdanlin area of southern Tibet (Figure 1); these rocks constitute the northernmost and probably earliest preserved record of initial India-Asia collision [*Ding et al.*, 2005; *Hu et al.*, 2012; *Wu et al.*, 2014]. The new data allow for refinement of previous estimates of the timing of initial India-Asia collision. We then construct a simple palinspastic flexural model that ties together the IYS record with previously documented records in the Tethyan Himalaya [*Willems et al.*, 1996; *Zhu et al.*, 2005; *Najman et al.*, 2010; *Hu et al.*, 2012; *Zhang et al.*, 2012] and in the southern, frontal part of the Himalaya of Nepal [*DeCelles et al.*, 1998a, 1998b, 2004; *Najman et al.*, 2005].

2. Geological Setting of the Sangdanlin Section

The Sangdanlin section is located ~8 km south of the town of Saga, in south-central Tibet (Figure 1). This region is situated amidst the Indus-Yarlung suture zone, which formed as the Indian and Asian continental landmasses collided during early Cenozoic time [*Garzanti et al.*, 1987]. The suture zone comprises three tectonic domains [*Burg et al.*, 1987]:

1. The Gangdese magmatic arc, consisting of granitoid and intermediate volcanic rocks ranging in age from mid-Cretaceous to late Miocene [*Maluski et al.*, 1982; *Schärer et al.*, 1984; *Debon et al.*, 1986; *Yin and Harrison*, 2000; *Kapp et al.*, 2005]; Cretaceous-Paleocene components of the Gangdese arc are generally interpreted to represent the precollisional magmatic arc formed above the subduction zone between continental southern Asia and the Tethyan oceanic domain [*Allégre et al.*, 1984; *Yin and Harrison*, 2000].
2. South of the Gangdese arc lies the >5 km thick Gangdese forearc basin, ranging in age from Aptian through Paleocene, and filled with marine to nonmarine sedimentary rocks [*Einsele et al.*, 1994; *Wang et al.*, 2012; *Orme et al.*, 2014] deposited upon ophiolitic subforearc basement [*Girardeau et al.*, 1984; *Guilmette et al.*, 2008, 2009; *Hébert et al.*, 2011].
3. South of the forearc basin lies the accretionary prism, composed of mud- and serpentinite-matrix mélanges, radiolarites, pillow basalts, and deep-marine sedimentary and metasedimentary rocks that accreted onto the southern margin of Asia as Tethyan oceanic lithosphere was subducted northward [*Girardeau et al.*, 1984; *Burg and Chen*, 1984; *Einsele et al.*, 1994; *Dürr*, 1996; *Ding et al.*, 2005; *Cai et al.*, 2012].

The Sangdanlin section was mapped by *Ding et al.* [2005] as resting conformably upon Cretaceous strata of the northern Tethyan Himalayan zone. These authors mapped the section as part of a large southward overturned footwall syncline beneath a north dipping thrust fault belonging to the Zhongba-Gyangze thrust system (Figure 1b). Faults of the Zhongba-Gyangze thrust system carry mélange and pillow basalt in their hanging walls and represent the southern boundary zone of the accretionary prism. This interpretation places the Sangdanlin section on top of the Cretaceous Jiabula Formation, which represents the northern Tethyan passive margin succession and implies that the section was deposited upon Indian continental or transitional lithosphere. In a contrasting interpretation, *Wang et al.* [2011] mapped the Sangdanlin section as completely bounded by faults and embedded within the mélanges. This interpretation isolates the Sangdanlin section from Indian lithosphere. In a third interpretation provided by the 1:250,000 geological map by *Yang et al.* [2003], the Sangdanlin section is in the hanging wall of a north dipping thrust fault that places Triassic, Jurassic, and Cretaceous Tethyan strata on top of the Jiabula Formation (Figure 1b). The Sangdanlin section is part of an approximately 10 km long (east-west) fault-bounded block that also includes the underlying Cretaceous section (Figure 1b) and lies beneath a southward verging thrust fault that carries Jurassic strata. This interpretation places the Sangdanlin section within the Zhongba-Gyangze thrust system, structurally below and above rocks that have Tethyan affinity.

A moderately northward dipping, homoclinal panel of phyllite, sandstone, slate, and phacoidal impure limestone of the Cretaceous Zhongzuo, Zheba, and Jiabula Formations can be followed southward from the Sangdanlin section for more than 5 km. *Yang et al.* [2003] mapped a pair of faults in this succession (Figure 1b), whereas *Ding et al.* [2005] mapped the succession south of the Sangdanlin section as a simple, north dipping limb of a large anticline. Unfortunately, the basal contact of the Sangdanlin section is buried beneath alluvium. However, based on the absence of obvious mélange material south of the section, we follow the interpretations of *Ding et al.* [2005] and *Yang et al.* [2003] in placing the Sangdanlin section at the top of the Tethyan succession and therefore on the continental part of the Indian plate. We emphasize, however, that until further geological mapping places the Sangdanlin section within an unequivocal geological context, the question of whether it originally rested upon oceanic or Indian continental lithosphere remains open.

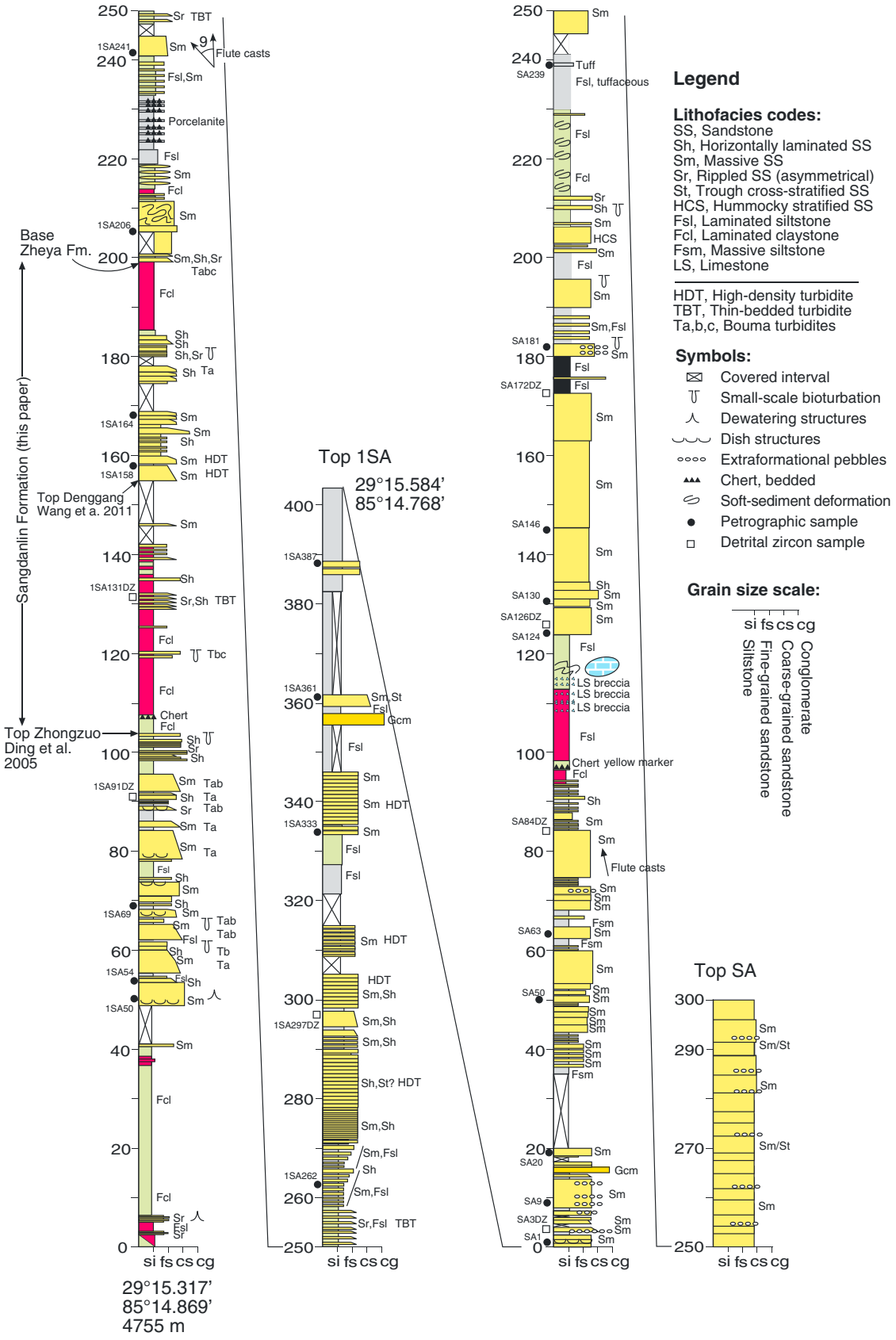

Figure 2. Measured stratigraphic sections of the Denggang (Zhongzuo), Sangdanlin, and Zheya Formations at Sangdanlin.

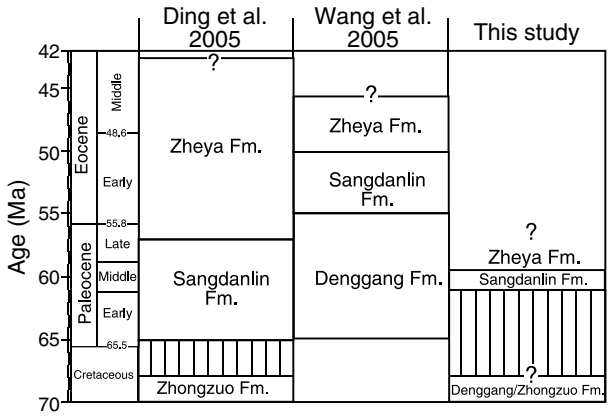

Figure 3. Chart showing nomenclature for stratigraphy of the Sangdanlin section from previous work and this study. Question marks indicate uncertain boundaries.

Based on paleontological ages and U-Pb dates on detrital zircons, the Sangdanlin section as a whole spans from Late Cretaceous to early Eocene time [*Ding*, 2003; *Ding et al.*, 2005; *Wang et al.*, 2011; *Wu et al.*, 2014]. Our new data (presented below) combined with previously reported paleontological ages indicate that the section ranges in age from Maastrichtian through Paleocene.

3. Sedimentology

Two stratigraphic sections covering the exposed thickness of the Sangdanlin succession were measured at a bed-by-bed level of detail and logged at 1:100 scale (Figure 2). Section 1SA covers the lower 403 m of the succession, and Section SA covers the upper 303 m of the section. The two sections were correlated a few hundred meters along strike by walking out marker beds. Exposure is generally excellent, such that details of sedimentary texture and structure are visible in outcrop. Samples were collected for sedimentary petrology and detrital geochronology.

The stratigraphic nomenclature of units exposed in the Sangdanlin section is discussed by *Ding* [2003], *Ding et al.* [2005], and *Wang et al.* [2011]. Both sets of authors divided the section into three formations: the Zhongzuo [*Ding*, 2003] or Denggang [*Wang et al.*, 2011], Sangdanlin, and Zheya Formations (Figure 3). *Ding* [2003] and *Ding et al.* [2005] used the term Zhongzuo Formation for the lowest formation, but *Wang et al.* [2011] noted that the Zhongzuo Formation was named for a lithologically distinct unit cropping out nearly 400 km east of Sangdanlin near Gyangze and coined a new local name for this interval—the Denggang Formation. We employ the terminology of *Wang et al.* [2011] but refer parenthetically to the *Ding et al.* [2005] terminology. We agree with *Ding et al.* [2005] in placing the contact between the Denggang (Zhongzuo) and overlying Sangdanlin Formations at the top of the first high cliff in the section, where the major lithology changes abruptly from massive quartzose sandstone to laminated green chert and siliceous mudstone (Figures 2, 4a, and 4d). *Ding et al.* [2005] considered this contact to be a disconformity representing the upper Maastrichtian. Based on the first appearance of Eocene-age detrital zircons, *Wang et al.* [2011] placed the contact between the Denggang (Zhongzuo) and Sangdanlin Formations ~50 m higher in the section, at about the 155 m level of our measured section (Figure 2). We prefer the contact placement of *Ding et al.* [2005], at the top of the thick stack of coarse-grained sandstone beds. This lithological break, from massive sandstone to laminated chert, is easily mappable in the field, is supported by paleontological data [*Ding et al.*, 2005], represents a major change in depositional environment, and is confirmed by sandstone modal petrographic data [this study; *Wang et al.*, 2011] and detrital zircon geochronology [this study].

Both *Wang et al.* [2011] and *Ding et al.* [2005] concur in their placement of the contact between the Sangdanlin and overlying Zheya Formations at the top of a predominantly red and green fine-grained interval corresponding roughly to the 200 m level of our measured section. Above this level, sandstone becomes increasingly prevalent in the section (Figure 2).

3.1. Denggang (Zhongzuo) Formation

The Denggang (Zhongzuo) Formation consists of 104 m of siliceous shale, chert, and sandstone. The unit includes a lower fine-grained interval and an upper sandstone-rich interval. The lower fine-grained interval consists of 49 m of green (predominantly) and red laminated shale and siltstone, with local radiolarian chert and siliceous claystone layers. Several beds of very fine- to fine-grained, green, rippled sandstone with dewatering structures are present in the lower 6 m of the section, but the bulk of the interval is monotonously fine-grained.

The upper, sandy unit comprises about 54 m of interbedded medium- to very coarse-grained quartzose sandstone with thin, laminated siltstone intercalations (Figure 4a). The sandstone beds are 1.5–6 m thick,

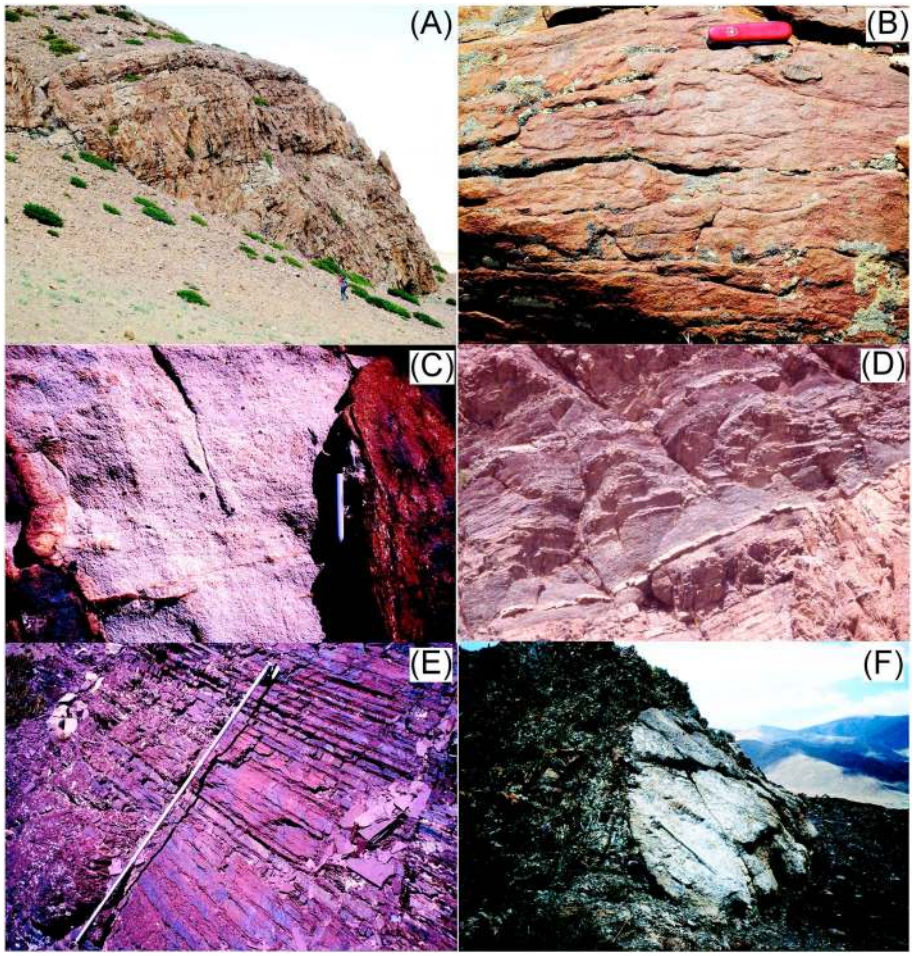

Figure 4. Photographs of Sangdanlin section lithofacies. (a) Stacked sandstones forming the massive cliff in upper half of Denggang (Zhongzuo) Formation, viewed from southwest. (b) Dish structures in Denggang (Zhongzuo) Formation. (c) Poorly sorted massive sandstone lithofacies, typical of turbidite facies S2 [*Lowe*, 1982] and F4, F5, and F7 [*Mutti*, 1992]. (d) Contact between the Denggang (Zhongzuo) and Sangdanlin Formations, viewed from south. (e) Red radiolarian chert of the Sangdanlin Formation. (f) Olistolith of Paleozoic fossiliferous limestone in Zheya Formation, viewed from west.

tabular with erosional but flat bases, and consist mainly of massive, upward fining, very coarse- to medium-grained sandstone. Thin granular to pebbly layers are present in the basal parts of several of these sandstone beds. Dish structures (Figure 4b) and wispy horizontal laminations are locally present, but most of the sandstone lacks primary sedimentary structures (Figure 4c). The upper parts of these thick sandstone beds commonly contain horizontal laminations and ripple cross-laminations and are capped by 0.5–1 m thick intensely bioturbated fine-grained sandstone layers. The blocky-weathering several-meter-thick sandstone beds are separated by thin (10–40 cm thick), laminated, gray siltstone layers. Also present are decimeter-thick beds of upward fining sandstone (coarse- or medium-grained to fine-grained) with horizontal laminations and ripple cross-laminations. Between the 97.5 and 103.5 m levels of the measured section (Figure 2), a series of thin sandstone beds with horizontal laminations and ripple cross-laminations alternate with thin mudstone drapes.

The sandy lithofacies in the Denggang (Zhongzuo) Formation can be classified and interpreted according to classic fine-grained and coarse-grained turbidite lithofacies schemes [e.g., *Bouma*, 1962; *Walton*, 1967; *Mutti and Ricci Lucchi*, 1975; *Lowe*, 1982; *Mutti*, 1992; *Talling et al.*, 2012]. The relatively thick, coarse-grained sandstone beds are typical examples of *Lowe*'s [1982] S1, S2, and S3 turbidite lithofacies and *Mutti*'s [1992] turbidite facies F4, F5, F7, and F8. These lithofacies are interpreted as the deposits of high-density turbidity flows, in which development of bed forms is suppressed by rapid sediment fallout rates [*Lowe*, 1982; *Talling et al.*, 2012]. Noting that these types of flows may not be turbidity flows sensu stricto, *Mulder and Alexander* [2001] suggested the term "concentrated density flows." In any case, these beds likely were deposited by

turbulent density flows with very high concentrations of sand. Stratification is rare in such deposits, owing to rapid deposition and dewatering/fluidization [*Talling et al.*, 2012]. Fluid escape produced dish structures [*Lowe and LoPiccolo*, 1974] and probably obliterated some sedimentary structures. Pebbly granular layers probably resulted from the development of traction carpets (*Lowe*'s [1982] lithofacies S2; *Mutti*'s [1992] F7). The relatively thin, finer-grained, rippled, and horizontally laminated upper parts of these sandstone beds can be classified as Bouma Tb and Tc turbidite intervals, respectively. These were deposited from the low-concentration tails of higher-density turbidity or concentrated density flows represented by the thick coarse-grained sandstone beds [e.g., *Lowe*, 1982; *Mutti*, 1992; *Mulder and Alexander*, 2001].

The assemblage of lithofacies in the upper 54 m of the Denggang (Zhongzuo) Formation is characteristic of sandy lobe deposits of turbidite fan systems [*Walker*, 1975; *Mutti et al*., 1978; *Bouma et al*., 1985; *Mutti*, 1992]. The uppermost part of the interval (97.5–103.5 m) consists of much finer-grained deposits with mudstone drapes, perhaps representing channel levee deposits [*Walker*, 1985; *Weimer*, 1989]. *Wang et al.* [2011] also interpreted the sandstone interval in the Denggang (Zhongzuo) Formation as turbidites.

3.2. Sangdanlin Formation

The Sangdanlin Formation is a total of 96 m thick. Its contact with the underlying Denggang (Zhongzuo) Formation is a sharp lithological break, from medium-grained horizontally laminated and rippled sandstone below, to bright green, siliceous, laminated shale above (Figure 4d). Three meters above the base, the Sangdanlin Formation becomes dominated by laminated, red siliceous shale and radiolarian chert (Figure 4e) [*Ding et al*., 2005]. The shale/chert-dominated interval continues for nearly 100 m upsection, and from that level upward sandy lithofacies become increasingly abundant in the Sangdanlin Formation. The most important lithofacies include rippled and horizontally laminated fine- to medium-grained sandstone; horizontally laminated to massive very coarse- to medium-grained sandstone; and green, gray, and red laminated siliceous shale and porcelanite. Massive, structureless sandstone beds occur in two basic modes: (a) 2–4 m thick beds with crude upward fining grain-sized trends, which are present in the middle part of the formation, and (b) 5–7 m thick massive sandstone beds in upward thickening and coarsening packages; these tend to be concentrated in the upper 45 m of the formation (Figure 2). Soft-sediment deformation is locally abundant in sandstones of the Sangdanlin Formation.

We interpret the siliceous shale and radiolarian cherts in the Sangdanlin Formation as the results of pelagic biogenic silica deposition [see also *Ding et al*., 2005; *Wang et al*., 2011]. The near absence of siliciclastic material in this part of the section suggests that the basin was temporarily isolated from the influx of clastic material. Sandstones in the upper 50 m of the formation include lithofacies similar to those documented in the Denggang (Zhongzuo) Formation, which were probably deposited by medial to distal turbidity currents.

3.3. Zheya Formation

The Zheya Formation rests conformably on top of the Sangdanlin Formation and is at least 501 m thick. The upper limit of the Zheya Formation is a thrust contact (Figure 1), such that its original total thickness is unknown. The Zheya-Sangdanlin contact is placed at the base of an upward fining sandstone bed at the 199.5 m level of our measured section. The background fine-grained lithology changes from red and green siliceous shale and radiolarian chert below this sandstone bed to predominantly gray shale, siliceous shale, and porcelanite above (Figure 2) [*Ding et al*., 2005].

Lithologies in the Zheya Formation are more variable than those in the underlying units, including fine-grained siliceous rocks, medium- to coarse-grained sandstones, and disrupted and olistostromal beds (Figure 4f). Overall, grain size coarsens upward (Figure 2). The lowermost part of the Zheya Formation comprises massive medium- to coarse-grained sandstone beds, with abundant large-scale penecontemporaneous deformation (200–212 m level) and disrupted sandstone layers (212–218 m level), overlain by white porcelanite beds. Above this zone lies a 110 m succession of massive and horizontally laminated sandstone beds, many with normal grading, and some stacked in upward thickening and coarsening packages on the order of 5–10 m thick. The sandstone packages are separated by gray, laminated siltstone and shale intervals. Some thin beds (e.g., 250–258 m levels) consist of fine-grained sandstone with ripple cross-laminations and mudstone drapes. From the 346 to 404 m levels, the section is dominated by gray laminated siltstone and shale. The upper ~300 m of the measured section contain four packages of medium- to coarse-grained sandstone with occasional beds of pebbly conglomerate. These four sandstone packages are separated from each other by 15–30 m thick intervals of red, gray, and green siliceous shale with some thin beds of radiolarian chert.

Table 1. Modal Petrographic Point-Counting Parameters[a]

Symbol	Description
Qm	Monocrystalline quartz
Qp	Polycrystalline quartz
Qpt	Foliated polycrystalline quartz
Qms	Monocrystalline quartz in sandstone or quartzite lithic grain
C	Chert
S	Siltstone
Qt	Total quartzose grains (Qm + Qp + Qpt + Qms + C + S)
K	Potassium feldspar (including perthite, myrmekite, and microcline)
P	Plagioclase feldspar (including Na and Ca varieties)
F	Total feldspar grains (K + P)
Lvm	Mafic volcanic grains
Lvf	Felsic volcanic grains
Lvv	Vitric volcanic grains
Lvx	Microlitic volcanic grains
Lvl	Lathwork volcanic grains
Lv	Total volcanic lithic grains (Lvm + Lvf + Lvv + Lvx + Lvl)
Lsh	Mudstone
Lph	Phyllite
Lsm	Schist (mica schist)
Lc	Carbonate lithic grains
Lm	Total metamorphic lithic grains (Lph + Lsm + Qpt)
Ls	Total sedimentary lithic grains (Lsh + Lc + C + S + Qms)
Lt	Total lithic grains (Ls + Lv + Lm + Qp)
L	Total nonquartzose lithic grains (Lv + Ls + Lph + Lsm + Lc)

[a]Accessory minerals (in decreasing order from most abundant): Muscovite, chlorite, epidote/zoisite, magnetite, tourmaline, biotite, cordierite, and zircon.

Bedding within the sandstone packages is 0.5–15 m thick (the thicker beds are probably amalgamated). Beds are tabular over hundreds of meters laterally, and lithofacies include massive, horizontally laminated, and rippled sandstone. Grain size ranges between pebbly and fine-grained sand. Granular to pebbly stringers and horizontal stratification are common. Flute and groove casts are present on the bases of a few beds. Disrupted stratification, boudinaged beds, and large blocks of extraformational fossiliferous carbonate rocks are present (Figure 4f). The uppermost part of the measured section is composed of massive and cross-stratified, poorly sorted, medium- to coarse-grained, micaceous sandstone. A tuffaceous horizon is present at the 643 m level of the composite measured section.

Although the variety of lithofacies present within the Zheya Formation is much greater than that within the Denggang and Sangdanlin Formations, the assemblage of physical processes responsible for deposition is similar. Most of the sandstone beds may be interpreted as various types of density current deposits (*Lowe*'s [1982] S2 and S3 and *Mutti*'s [1992] F5, F7, and F8 turbidite facies). The sandstone packages in the upper several hundred meters of the Zheya Formation may be interpreted as turbidite sandstone lobes, deposited by laterally expanding turbidity currents on the middle to outer parts of submarine fans [e.g., *Normark*, 1978; *Mutti and Normark*, 1991; *Mutti*, 1992; *Gervais et al.*, 2006]. Background fine-grained sedimentation was dominated by pelagic fallout.

3.4. Paleocurrent Directions

We obtained paleocurrent data from sparse flute casts at the ~240 m and 480 m levels, which indicate generally north-northwestward paleoflow direction. *Ding et al.* [2005] reported paleocurrent data from cross-stratification in the Denggang (Zhongzuo) Formation that demonstrate northward paleoflow and data from the Zheya Formation showing south-southwestward paleoflow. We did not observe cross-stratification in the Denggang (Zhongzuo) Formation.

4. Petrographic Data

4.1. Previous Work

Petrographic data from the Sangdanlin section presented by *Wang et al.* [2011] showed that Denggang (Zhongzuo) Formation sandstones are characterized by hyper-quartzose compositions, whereas sandstones in the overlying Sangdanlin and Zheya Formations contain abundant volcanic lithic grains and feldspars. Spinel is present in Sangdanlin and Zheya Formation sandstones but not in the Denggang (Zhongzuo) Formation. The spinel has high Cr [Cr/(Al + Cr) > 0.4] and low TiO_2 wt % [*Ding et al.*, 2005; *Wang et al.*, 2011].

4.2. Methods

Twenty-nine samples of medium-grained sandstone were collected in the field and cut for standard petrographic thin sections in order to generate modal petrographic data for provenance analysis. Each thin section was stained for K-feldspar and Ca-plagioclase, and 450 framework grains were counted according to a modified version of the Gazzi-Dickinson point-counting method. Grain types and modal parameters are listed and defined in Table 1. Recalculated data are presented in Table 2.

Table 2. Recalculated Modal Petrographic Point-Count Data

SAMPLE	Qm%	F%	Lt%	Qt%	F%	L%	Qm%	P%	K%	Lmet%	Lv%	Lsed%
1SA54	93	1	6	98	1	1	99	1	0	33	17	50
1SA55	91	0	9	99	0	1	100	0	0	6	6	89
1SA69	93	0	7	99	0	1	100	0	0	13	0	87
1SA94	96	0	4	100	0	0	100	0	0	0	0	100
1SA131	47	19	34	56	19	26	71	29	0	23	59	18
1SA164	95	0	5	99	0	1	100	0	0	10	0	90
1SA206	48	30	22	55	29	16	61	39	0	12	71	18
1SA262	38	28	34	46	28	26	58	42	0	9	64	28
1SA297	51	23	26	58	23	19	69	31	0	10	82	8
1SA361	51	13	36	59	13	28	80	20	0	17	51	32
1SA387	53	9	37	59	9	32	85	15	0	14	60	27
SA1	43	27	30	48	27	25	62	38	0	6	82	12
SA3	46	27	27	50	27	22	63	37	0	9	79	11
SA9	46	26	27	53	26	21	64	36	0	8	78	14
SA20	48	25	26	55	25	20	65	35	0	10	77	13
SA50	39	29	31	48	29	23	57	43	0	16	68	16
SA63	39	30	31	46	29	25	56	44	0	18	65	17
SA75	33	34	33	40	33	27	49	51	0	14	77	9
SA124	40	21	39	51	20	29	66	34	0	22	61	17
SA130	43	28	29	51	27	21	60	40	0	15	69	15
SA146	40	29	31	45	29	26	58	42	0	17	72	11
SA172	43	23	34	55	23	23	66	34	0	16	65	20
SA181	41	25	34	51	24	25	62	38	0	17	54	30
SA202	43	19	37	57	19	24	69	31	0	15	56	29
SA241	43	27	30	52	26	21	61	39	0	12	67	20
SA247	49	29	22	60	29	11	63	37	0	13	57	29
SA254	43	25	32	54	24	21	64	36	0	21	51	28

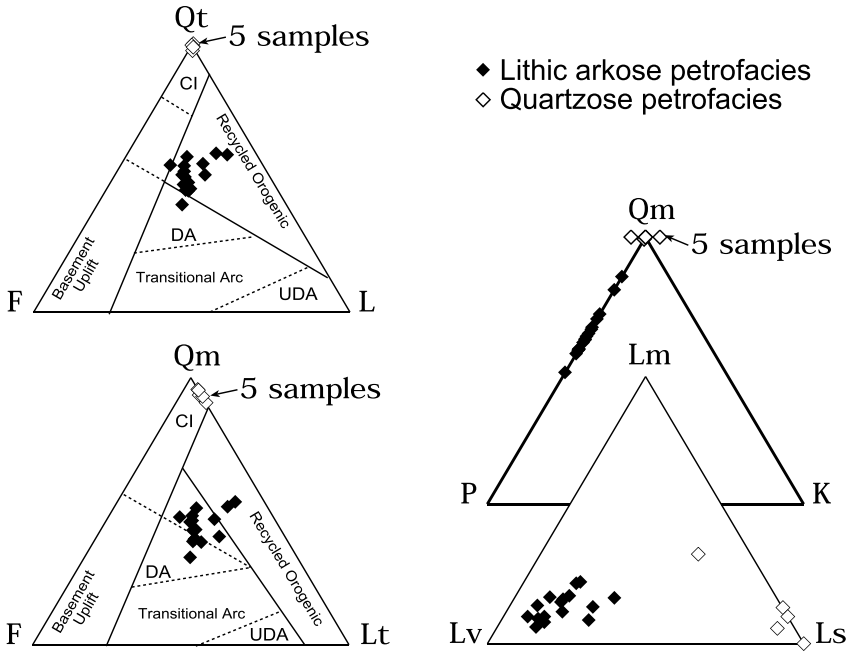

Figure 5. Ternary diagrams showing compositions of sandstones from the Sangdanlin section. See Figures 2 and 7 for sample locations. Provenance subfields are from *Dickinson et al.* [1983]. Abbreviations as follows: DA, dissected arc; UDA, undissected arc; CI, craton interior.

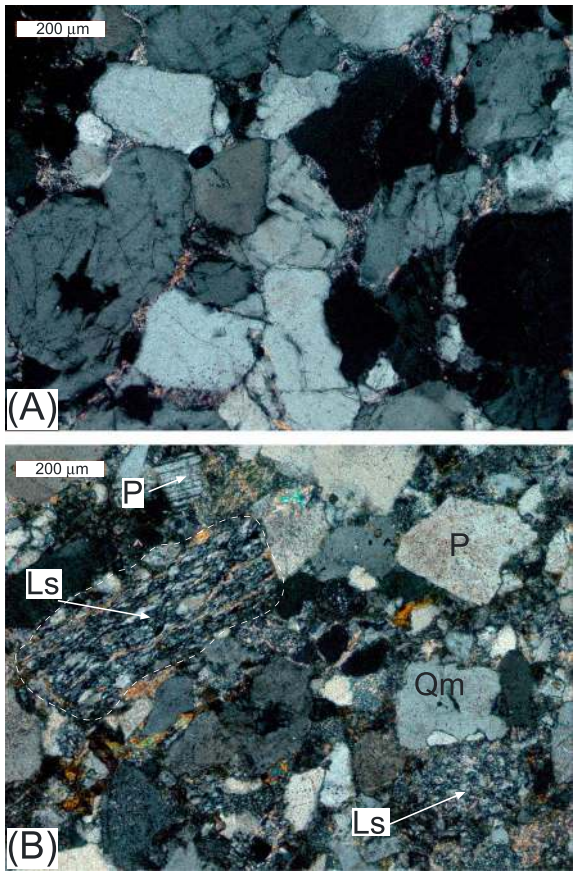

Figure 6. Photomicrographs of the (a) quartz-arenitic and (b) feldspatholithic petrofacies. The quartzose example is composed of 100% quartz (mainly Qm) grains; the feldspatholithic example contains plagioclase (P) and sedimentary lithic (Ls) grains, in addition to quartz.

4.3. Results

Principal grain types identified in the Sangdanlin section samples include monocrystalline quartz (Qm), polycrystalline quartz (Qp), foliated polycrystalline quartz (Qpt), monocrystalline quartz within recycled quartzose sedimentary lithic grains (e.g., quartzite; Qss), plagioclase (mainly calcic) feldspar (P), and various types of lithic grains, including low-grade metasedimentary (phyllite, mica schist, and marble), sedimentary (shale/argillite, limestone, and chert), and volcanic lithic grains. No K-feldspar grains were found. Volcanic lithic grains include microlitic, lathwork (trachytic), vitric, mafic, and felsic varieties (Table 1). Felsic volcanic grains consist of highly sericitized microcrystalline lithic grains. Mafic volcanic grains are epidote and/or pyroxene rich. Vitric grains are microcrystalline quartz, easily confused with chert were it not for their inclusion of feldspar microcrysts and glassy flow textures. Lathwork (trachytic) and microlitic grains are the most abundant volcanic grain types. Trace minerals include epidote, tourmaline, magnetite, zircon, muscovite, and a few unidentified opaque grains.

Modal petrographic data are plotted on standard ternary diagrams in Figure 5. The sandstone compositions fall into quartz-arenitic (Figure 6a) and feldspatholithic (Figure 6b) groups [*McBride*, 1963]. The quartz arenites are in the lower part of the section, mainly in the Denggang (Zhongzuo) Formation, and the feldspatholithic sandstones are in the Sangdanlin and Zheya Formations. Average compositions of sandstones in the Denggang (Zhongzuo) Formation are %QmFLt = 93, 1, 6; %QtFL = 98, 1, 1; %QmPK = 99, 1, 0; and %LmLvLs = 12, 4, 83. These compositions plot within the stable craton interior provenance field of *Dickinson et al.* [1983]. Average sandstone framework compositions for Sangdanlin and Zheya Formation samples are as follows: %QmFLt = 44, 25, 31; %QtFL = 52, 25, 23; %QmPK = 64, 36, 0; and %LsLvLm = 14, 67, 19. These plot in the dissected magmatic arc and recycled orogen provenance fields of *Dickinson et al.* [1983] (Figure 5). The abrupt compositional change from pure quartz arenites to feldspatholithic arenites takes place within the Sangdanlin Formation. The first occurrence of feldspatholithic petrofacies is at the 131 m level of the section, and the last occurrence of quartz arenite is at the 164 m level.

5. Detrital Zircons

5.1. Methods

Ten samples of medium- to coarse-grained sandstone were processed by standard methods for retrieving dense minerals, and detrital zircon grains were separated from these concentrates using heavy liquids. Zircons were mounted in epoxy, polished, and analyzed for U-Pb ages by laser ablation multicollector inductively coupled plasma mass spectrometry (LA-MC-ICPMS) at the University of Arizona LaserChron Center. The methods employed are described in *Gehrels et al.* [2008]. A total of 1125 detrital zircon grains produced data of sufficient precision for geochronological interpretation. Analyses that yielded isotopic data of acceptable discordance, in-run fractionation, and precision are listed in the supporting information Table S1. Because $^{206}Pb/^{238}U$ ages are generally more precise for younger ages, whereas $^{206}Pb/^{207}Pb$ ages are more precise for

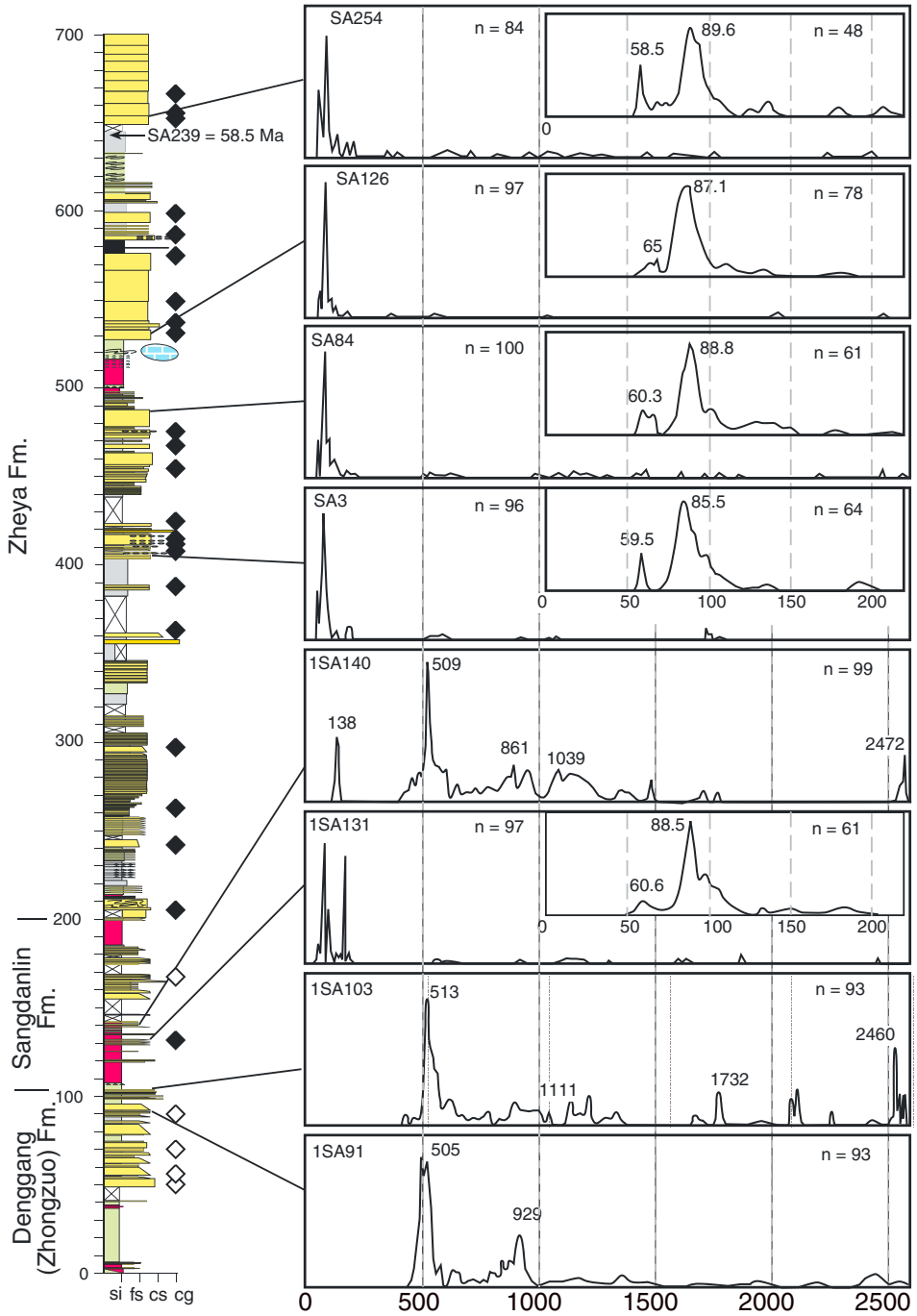

Figure 7. Detrital zircon data from the Sangdanlin section, shown in normalized probability density diagrams. Inset plots show the <200 Ma ages only; *n* = number of grains.

older ages, we report $^{206}Pb/^{238}U$ ages up to 1000 Ma and $^{206}Pb/^{207}Pb$ ages if the $^{206}Pb/^{238}U$ ages are >1000 Ma [*Gehrels et al.*, 2008]. These analyses are plotted on relative age-probability diagrams (Figure 7), which represent a sum of the probability distributions of all analyses from a sample, normalized such that the areas beneath the probability curves are equal for all samples depicted in the figure. Age peaks on these diagrams are considered robust if defined by several analyses.

We also collected and processed a single sample for U-Pb geochronology from a tuffaceous layer at the 643 m level of the composite measured section (sample SA239; Figure 7). Clear euhedral zircons were picked,

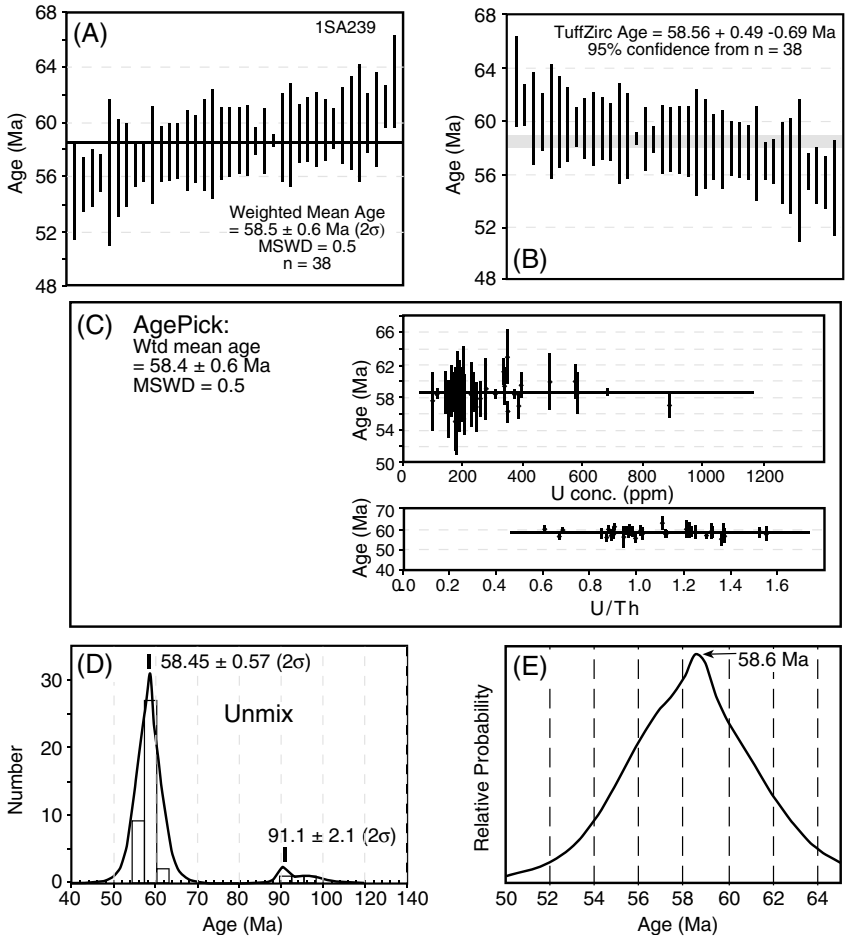

Figure 8. Mean age plots for sample SA239, a tuff from the Zheya Formation. (a) Standard weighted mean plot, (b) Tuffzirc age calculation, and (c) results of AgePick routine, showing U concentration and U/Th ratio. Note that both of the latter exhibit no trends with age, which suggests the presence of a single population in which Pb loss is not a problem. (d) Results of the Unmix routine, which identifies discrete populations and calculates their mean ages and uncertainties. (e) The age of the peak on the probability density function (38 crystals).

mounted in epoxy, polished, and analyzed for U-Pb ages by LA-MC-ICPMS at the LaserChron Center. Analytical data for sample SA239 are provided in the supporting information Table S1, and mean age plots are provided in Figure 8 and discussed in more detail in section 7.

5.2. Results

The detrital zircon signatures of sandstones in the Sangdanlin section fall into two mutually exclusive categories (Figure 7). Two samples from the Denggang (Zhongzuo) Formation (1SA91 and 1SA103) exhibit prominent age distribution peaks in the ~490–520 Ma (mean peak at 505 Ma) and ~800–960 Ma (mean peak at 929 Ma) ranges. Older grains in the 1.0–1.5 Ga and 2.4–2.5 Ga ranges are also present. No grains younger than 490 Ma are present in these two samples.

One sample from the Sangdanlin Formation (1SA140) exhibits zircon ages similar to those from the Denggang (Zhongzuo) Formation samples, with the addition of a strong peak at circa 138 Ma (Figure 7). The other sample from the Sangdanlin Formation (1SA131) is similar to all the remaining samples that were collected upsection in the Zheya Formation. These samples are dominated by detrital zircon age distribution peaks in the $<$200 Ma age range (Figure 7). More than 65% of the grains analyzed in these samples are younger than 200 Ma. Two prominent age peaks occur at circa 90–80 Ma and 65–58 Ma, with subsidiary poorly defined peaks in the 200–125 Ma range. The pre-200 Ma zircons in these samples exhibit clusters in the circa 500 Ma and 900–1200 Ma age ranges. Archean grains are also present in small quantities in these samples.

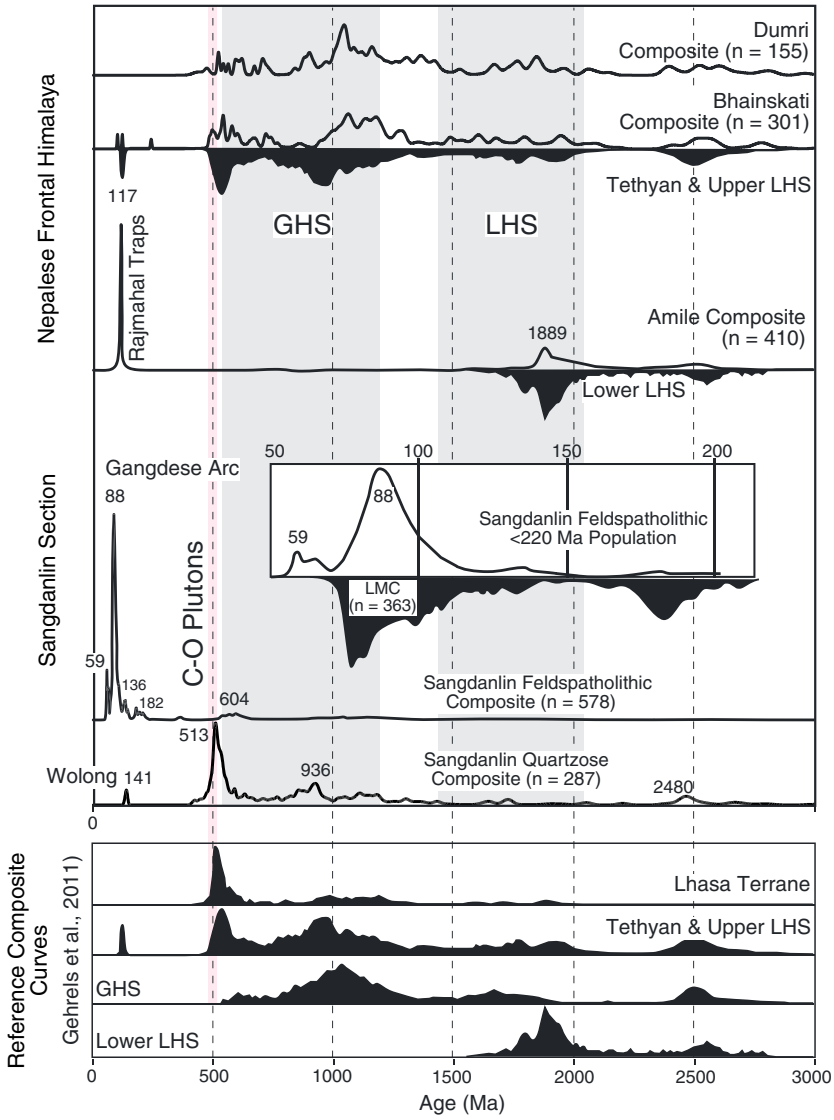

Figure 9. Comparisons of probability density functions for detrital zircon ages from the Sangdanlin area [this study]. (bottom) Reference populations from Himalayan terranes and the Lhasa terrane [*Gehrels et al.*, 2011], and (top) age populations from Nepal [*DeCelles et al.*, 2004; this study]. Gray rectangles highlight age ranges typical of the Greater Himalayan (GHS) and Lesser Himalayan (LHS) sequences in Nepal. Pink line labeled "C-O plutons" highlights ages from Cambrian-Ordovician plutons in the Greater Himalayan sequence that were recycled into Tethyan Himalayan strata. Note that the "Tethyan and upper LHS" composite reference curve includes zircons from the Permian, Cretaceous, and Paleocene strata of the thrust belt in southern Nepal. In the Sangdanlin section, the detrital zircon populations change from the Quartzose petrofacies to the Feldspatholithic petrofacies; in Nepal, the change occurs between the Paleocene Amile Formation and the middle Eocene Bhainskati Formation. The Lhasa terrane magmatic composite curve (LMC, shown in black and mirrored downward beneath the <220 Ma population from the Sangdanlin feldspatholithic group) is after *Cai et al.* [2012]. See text for discussion.

Two samples from the Cretaceous(?)-Paleocene Amile Formation from the Dumri Bridge section in the Lesser Himalaya of central Nepal (Figure 1) (see *DeCelles et al*. [2004, Figure 5] for stratigraphy of the Dumri Bridge section) also were processed for detrital zircon U-Pb ages. These samples produced Paleoproterozoic and Archean age clusters and a prominent ~117 Ma peak (Figure 9). These data are consistent with previously reported detrital zircon ages from the Amile Formation at the Dumri Bridge section [*DeCelles et al.*, 2004] and provide further constraints on the regional foreland basin evolution of the Himalaya as discussed below.

6. Provenance Interpretation

Sandstones in the Denggang (Zhongzuo) Formation are compositionally hypermature, reflecting derivation from a stable, highly weathered source terrane or recycling of quartzose sedimentary rocks. On the other hand, the Denggang (Zhongzuo) Formation sandstones are texturally immature, with poor sorting and grain-sized up to granular and pebbly sand. Coupled with sedimentological evidence discussed above, the compositionally mature, texturally immature aspect of these sandstones suggests that the sediment originated in a deeply weathered terrane and was transported rapidly by concentrated density flows or turbidity flows into a deep-marine setting, without significant storage time in nearshore and shelf settings.

In contrast to the Denggang (Zhongzuo) Formation, Sangdanlin and Zheya Formation sandstones exhibit immature textures and compositions. The abundance of trachytic volcanic lithic grains and calcic plagioclase (and the absence of K-feldspar) indicates the presence of basaltic to andesitic rocks in the source terrane. Limited quantities of metasedimentary lithic grains such as phyllite, mica schist, quartzite, and marble indicate local low-grade metasedimentary sources.

The petrographic data strongly implicate a drastic change in sediment provenance, from a hypermature, deeply weathered source terrane during deposition of the Denggang (Zhongzuo) Formation to a nearby topographically elevated, orogenic source terrane during deposition of the Sangdanlin and Zheya Formations. The compositional change is located between the 131 and 164 m levels of our composite measured section [see also *Wang et al.*, 2011]. The fact that feldspatholithic and quartz-arenitic sandstones alternate within this ~30 m part of the section indicates that the change in source areas was gradual and that the same depositional area received sediment from both source terranes over a period of time.

Potential sources of detritus in the Sangdanlin section as a whole include the Tethyan Himalaya, rocks of the accretionary prism, recycled Xigaze Group forearc strata, and the Gangdese magmatic arc (Figure 9). The northern part of the Tethyan Himalaya is composed of fine-grained siliciclastic and carbonate rocks that were deposited during Triassic through Cretaceous time along the northern passive margin of Greater India [e.g., *Gaetani and Garzanti*, 1991]. The accretionary prism consists of south verging, imbricated thrust sheets of Triassic, Jurassic, and Cretaceous pelagic chert, mudstone, mafic volcanic rocks (basalt, diabase, and gabbro), and ultramafic rocks (harzburgite and dunite), along with blocks of limestone and sandstone. These lithologies are distributed among mud-matrix, serpentinite-matrix, and chert-matrix mélanges [*Girardeau et al.*, 1984; *Guilmette et al.*, 2009; *Cai et al.*, 2012]. The Gangdese magmatic arc is composed of granitoid and intermediate volcanic cover rocks (mainly andesites, dacites, and pyroclastic and epiclastic rocks [*Debon et al.*, 1986; *He et al.*, 2007]). The Xigaze Group contains conglomerates, feldspatholithic sandstones, and shales [*Wang et al.*, 2012; *Orme et al.*, 2014].

General absence of serpentinitic, mafic, and ultramafic framework grains suggests that the ophiolitic portion of the accretionary prism was not a major source of detritus for any of the strata exposed in the Sangdanlin section. Abundant plagioclase and volcanic lithic grains above the ~130 m level of the section implicate sources in the Gangdese arc and/or Xigaze forearc. However, the absence of K-feldspar in these sandstones implies that the plutonic core of the Gangdese arc remained buried. Low-grade metasedimentary and sedimentary detritus could have been derived from either the Tethyan Himalaya or from the forearc side of the system. *Ding et al.* [2005], *Wang et al.* [2011], and *Wu et al.* [2014] inferred that the quartzose Denggang (Zhongzuo) Formation was derived from Tethyan Himalayan sources and the Sangdanlin and Zheya Formations were derived from the Asian side of the basin. Detrital zircon U-Pb geochronology provides a simple test of this hypothesis and sheds light on details of the initial India-Asia collision process.

The detrital zircon U-Pb results are remarkably consistent with the sandstone petrographic data. The Denggang (Zhongzuo) Formation sandstones contain Early Cretaceous and pre-490 Ma zircons, and their age distributions mirror those of documented Tethyan Himalayan zircons (Figure 9) [*DeCelles et al.*, 2000; *Hu et al.*, 2010; *Gehrels et al.*, 2011]. In contrast, zircon age data from the Sangdanlin and Zheya Formations show clearly that sources in the Gangdese magmatic arc were dominant. The Gangdese arc experienced major flare-ups during the Late Cretaceous (circa 90–75 Ma) and Latest Cretaceous-Eocene (circa 68–48 Ma) [*Schärer et al.*, 1984; *Xu et al.*, 1985; *Coulon et al.*, 1986; *Debon et al.*, 1986; *Copeland et al.*, 1995; *Ding*, 2003; *Lee et al.*, 2009; *Chung et al.*, 2005, 2009; *He et al.*, 2007]. Both of these age ranges are strongly represented in the detrital zircon age data presented here and in *Wang et al.* [2011] and *Wu et al.* [2014]. This result is consistent with the abundance of volcanic lithic grains and plagioclase in Sangdanlin and Zheya Formation sandstones. Another potential source of detritus for the Sangdanlin and Zheya Formations is the Xigaze Group in the forearc basin,

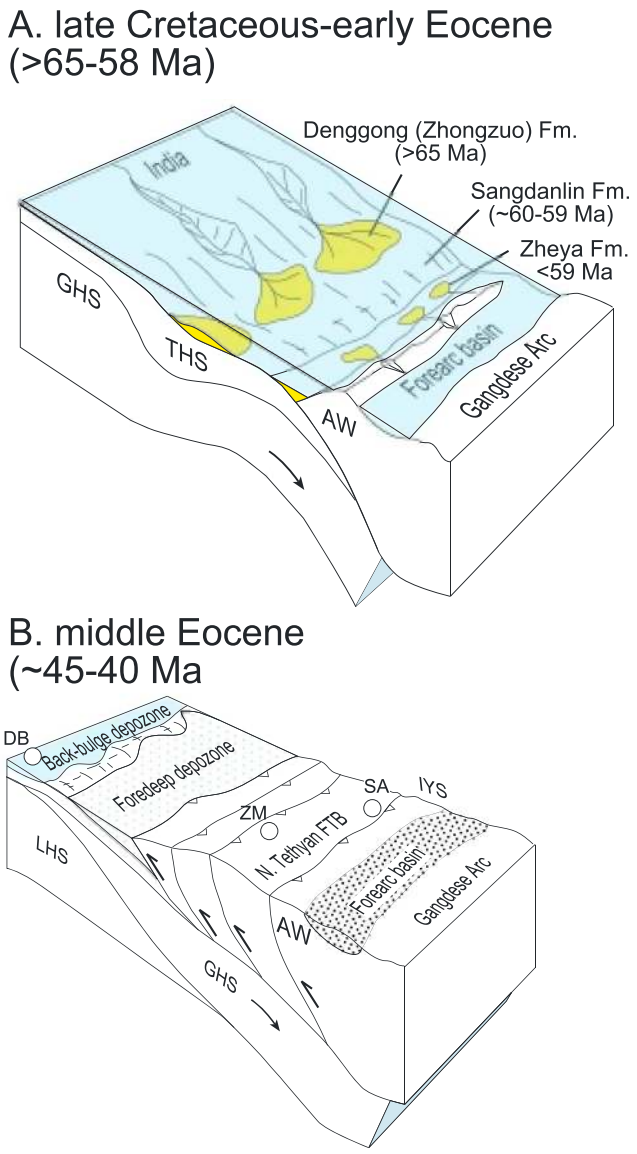

Figure 10. (a) Paleogeographic sketch of the Indus-Yarlung suture zone during deposition of Sangdanlin section. Note that various portions of the sketch refer to paleogeographic setting of Sangdanlin area during different time frames, from Late Cretaceous to early Eocene. (b) Sketch of the nascent Himalayan thrust belt during middle Eocene time, when the Tethyan thrust belt was propagating southward and the Bhainskati Formation was being deposited in the back-bulge depozone of the distal foreland basin. Abbreviations for schematic locations: DB, Dumri Bridge in the Lesser Himalaya; ZM, Zhepure Mountain in the Tethyan Himalaya; SA, Sangdanlin section. IYS is the Indus-Yarlung suture zone; AW is the accretionary wedge.

which contains intermediate volcanic clasts and sandstones with feldspatholithic compositions, as well as detrital zircons with ages in the 89–54 Ma range [*Dürr*, 1996; *Orme et al.*, 2014]. However the forearc basin sandstones also contain small amounts of K-feldspar, which is completely absent from the Sangdanlin and Zheya Formations. Sangdanlin and Zheya Formation sandstones also are more quartzose than those of the Xigaze Group, suggesting that either the Sangdanlin section sandstones were slightly "cleaned up" as they were partially reworked from the Xigaze Group or they were not recycled.

On the bases of the petrographic and detrital geochronological data we suggest that the Denggang (Zhongzuo) Formation was derived principally from the Tethyan Himalaya and deposited in turbidite fans along the base of the northern continental slope of Greater India (Figure 10a). Sandstones of the Sangdanlin and Zheya Formations were mainly derived from the Asian side of the system and also accumulated in deep-marine environments (Figure 10a). The transition between these end-member settings is represented in the Sangdanlin Formation, which consists predominantly of radiolarian chert and was probably deposited under circumstances in which detrital input was strongly restricted, perhaps athwart the crest of a bathymetric high between adjacent bathymetric lows in which siliciclastic turbidites were accumulating.

7. Chronostratigraphy

Previous interpretations of the chronostratigraphy of the Sangdanlin section are illustrated in Figure 3. *Ding et al.* [2005] assigned ages to the strata in the Sangdanlin section as follows: the Denggang (Zhongzuo) Formation was attributed to the lower Maastrichtian based on planktonic foraminifera; the Sangdanlin Formation to the Paleocene (Danian to Thanetian, circa 65–57 Ma) using mainly radiolaria; and the Zheya Formation to latest Paleocene-middle Eocene (57–42 Ma). These authors suggested the presence of a disconformity at the base of the Sangdanlin Formation, representing roughly 5–7 Myr. *Wang et al.* [2011] cited late Campanian [*Li et al.*, 2007] and Paleocene [*Ding*, 2003] radiolarian fauna in the siliceous beds directly above the top of the Denggang (Zhongzuo) Formation (the ~105–110 m level of our section, Figure 2). Detrital zircon U-Pb ages and radiolaria reported from chert beds in the Sangdanlin Formation [*Li et al.*, 2007] led *Wang et al.* [2011]

to interpret an Ypresian age for the onset of Sangdanlin Formation deposition. These authors also suggested that the Zheya Formation may be middle Eocene or even younger based on a single detrital zircon U-Pb age of 49.1 ± 0.7 Ma in the upper part of the Zheya Formation.

Our U-Pb zircon age data exhibit prominent minimum age peaks in the 60–58 Ma range (Figure 7). These ages provide a robust maximum age of deposition for the Sangdanlin and Zheya Formations, but no zircons with ages approximating the depositional age of the Denggang (Zhongzuo) Formation were found. Zircons from a tuffaceous layer in the upper part of the Zheya Formation (at the 643 m level of the composite section) provide a new direct age constraint on the rocks of the Sangdanlin section (Figure 8). We reduced the U-Pb data from the tuff and calculated a best age by five different algorithms (Figure 8):

1. The weighted mean age calculated from the cluster of 38 youngest crystals is 58.5 ± 0.6 Ma (2σ), with an MSWD = 0.5.
2. The Tuffzirc algorithm, which extracts a "best" age by focusing on the tightest cluster of ages while rejecting younger ages compromised by Pb loss and older ages due to inheritance, produced a weighted mean age of 58.56 + 0.49 – 0.69 Ma (95% confidence) from the coherent group of 38 zircons.
3. The AgePick algorithm employs U concentration and U/Th ratios to assess the potential for Pb loss and the existence of discrete age subpopulations. U concentration and U/Th ratios are constant for the main 38-grain population, suggesting a single population not subject to Pb loss or inheritance. This approach yielded a weighted mean age of 58.4 ± 0.6 Ma with MSWD = 0.5.
4. The Unmix algorithm determines the best-fitting Gaussian distribution for multiple age clusters and calculates the mean age and uncertainty of each age group. This produced a mean age of 58.4 ± 0.57 Ma for the youngest population.
5. Finally, the peak age of the 38-grain population from the probability density function is 58.6 Ma. The consistency of all five approaches in producing an age of ~58.5 ± 0.6 Ma indicates that this is the likely age of the tuff sample. Together with the minimum age clusters provided by detrital zircon ages from sandstone samples (Figure 7), this tuff age limits the time of deposition of most of the Sangdanlin section between ~60 Ma and 58.5 Ma. This age range is similar to the age estimated by *Wu et al.* [2014] from detrital ages but several million years older than the ages interpreted by *Wang et al.* [2011] based on the youngest fractions of detrital zircon ages. However, the use of the youngest age fraction or the youngest single grain age in most detrital zircon data sets will almost always produce an erroneously young age [*Dickinson and Gehrels*, 2009].

8. Relationship With Nepal Paleogene and Flexural Model

Data from the Sangdanlin section may be combined with previous work in two other areas of Paleogene outcrop in the Himalaya to provide a holistic view of the Paleocene-Eocene evolution of the Himalayan orogenic belt and its associated foreland basin system. Paleogene sections that archive the transition from Indian passive margin sedimentation to deposition dominated by influx of sediment from the Asian margin and the early Himalayan thrust belt are preserved at Zhepure Mountain in the northern Tethyan Himalaya [*Zhu et al.*, 2005; *Najman et al.*, 2010; *Hu et al.*, 2012] and in the Lesser Himalaya of southern central Nepal [*DeCelles et al.*, 1998a, 2004; *Najman et al.*, 2005; *DeCelles*, 2012] (Figures 1 and 11). Zhepure Mountain is located ~50 km south (along strike to the east) of Sangdanlin, and the southern Nepalese sections are situated ~175 km farther south.

At Zhepure Mountain (also referred to as the Qumiba section) [*Najman et al.*, 2010], an assemblage of paleontological, sedimentary petrological, and detrital geochronological and thermochronological data demonstrates that the onset of Asian detrital influx took place at approximately 52–50 Ma, during deposition of the Enba and Zhaguo Formations (see *Najman et al.* [2010] and *Hu et al.* [2012] for detailed reviews). *DeCelles et al.* [2004], *Hu et al.* [2012], *Zhang et al.* [2012], and *DeCelles* [2012] suggested that the underlying Zongpu (or Zhepure Shan) Formation recorded the passage through this region of the flexural forebulge. Using similar sedimentological arguments, *Garzanti et al.* [1987] and *Green et al.* [2008] argued that a flexural forebulge migrated across the northwestern Indian Himalaya during late Paleocene-early Eocene time. At Zhepure Mountain, the Enba and Zhaguo Formations represent the basal foredeep at this latitude. Apatite fission track ages, reset by burial to depths of 4–6 km, imply that a thick foredeep succession was deposited

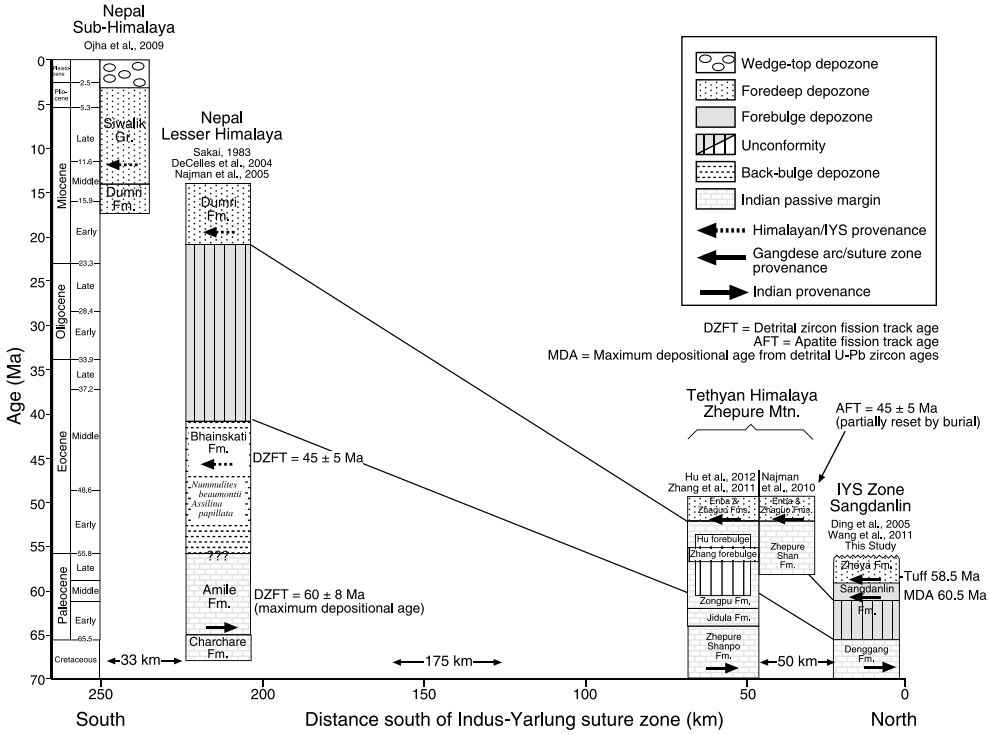

Figure 11. Diagram showing the relative locations (with respect to the Indus-Yarlung suture (IYS)) of the various stratigraphic records of India-Asia collision and subsequent foreland basin development. Sections are annotated with key age constraints and sources of information.

on top of the Enba-Zhaguo strata and subsequently eroded [*Najman et al.*, 2010]. In the Lesser Himalaya, the transition from Indian passive margin sedimentation to distal foreland basin deposition is indicated by an abrupt change of detrital zircon populations in the Paleocene Amile Formation and the middle Eocene (circa 45–40 Ma) Bhainskati Formation. Amile Formation detrital zircons exhibit U-Pb ages characteristic of Indian cratonic sources, whereas Bhainskati Formation detrital zircon ages are typical of Tethyan Himalayan strata (Figure 9) (*DeCelles et al.* [2004]; this study, samples DB2 and DB15, and Table S1 in the supporting information). The presence in the Bhainskati Formation of a circa 45 Ma population of detrital zircon fission track ages not reset by burial heating adds credence to the hypothesis that detritus was being supplied to the distal foreland from the nascent Tethyan Himalayan thrust belt by middle Eocene time [*Najman et al.*, 2005]. *Jain et al.* [2009] and *Ravikant et al.* [2011] arrived independently at a similar conclusion based on data from Eocene strata in the northern Indian Himalaya. A disconformity between middle Eocene and lower Miocene strata, marked by a prominent Oxisol horizon [*Sakai*, 1983], has been interpreted as the signal of forebulge passage through the Lesser Himalayan region during late Eocene-Oligocene time [*DeCelles et al.*, 1998a].

Figure 11 depicts the three sets of stratigraphic sections that are relevant to this discussion in their present geographic framework, along with key elements of each record. Palinspastic reconstruction of the Himalayan thrust belt is necessary to provide their Paleocene-Eocene relative locations. Shortening estimates derived from balanced cross sections in the central portion of the thrust belt range between about 600 km and 750 km [*DeCelles et al.*, 2001; *DeCelles et al.*, 2002; *Robinson et al.*, 2006; *Long et al.*, 2011]. *Murphy* [2007] reported Nd isotopic data from rocks exposed in the Gurla Mandhata core complex in the Tethyan Himalaya that require an additional 100–150 km of Lesser Himalayan shortening, which raises the total estimate to as much as 900 km. Because these values do not account for large amounts of penetrative strain in the rocks, they are probably significantly underestimated. Nevertheless, these estimates provide a starting point for a palinspastic flexural analysis of the Paleogene foreland basin system.

Flexural profiles for the northern Indian margin as it entered the subduction zone along southern Asia can be calculated by assuming values for the flexural rigidity of Indian lithosphere and the size of the growing Himalayan thrust belt load (Figure 12) [*Turcotte and Schubert*, 2006]. Because the age of Indian lithosphere

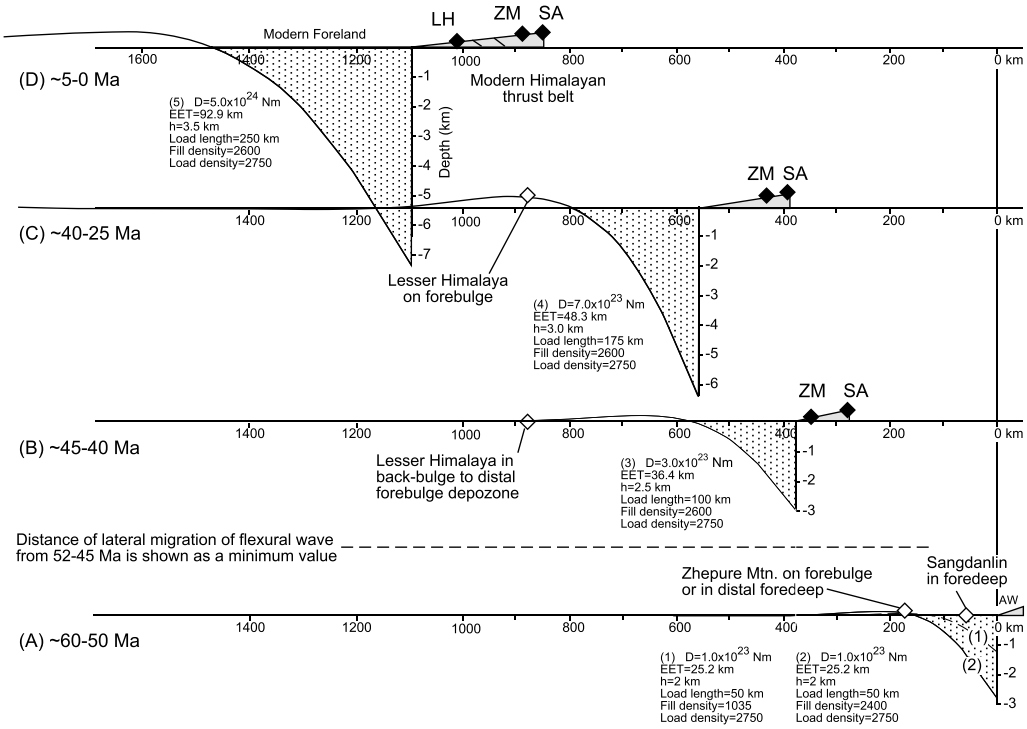

Figure 12. Palinspastic flexural model for the Paleocene-modern foreland basin system of the Himalayan orogenic belt. Horizontal axis is distance south of Indus-Yarlung suture. Parameters used in each model frame are listed (EET = effective elastic thickness, h = topographic height of load, and D = flexural rigidity). Two flexural profiles are provided in frame a, one for a sediment-filled basin and one for a water-filled basin. White diamonds show locations of Sangdanlin, Zhepure Mountain, and the Lesser Himalayan zone in approximate locations relative to the flexural profile at time of deposition; black diamonds show the same locations (SA, Sangdanlin; ZM, Zhepure Mountain; LH, Lesser Himalaya) after each was incorporated into the growing thrust belt. AW = accretionary wedge. Palinspastic distances are based on shortening estimates and kinematic histories from *DeCelles et al.* [2001], *Robinson et al.* [2006], and *Murphy* [2007]. Dashed horizontal line between frames a and b indicates time frame in which major uncertainty exists for Himalayan shortening.

entering the flexural profile through time has increased from Neoproterozoic to Archean over the course of the Himalayan orogeny [*DeCelles et al.*, 2002], it is likely that flexural rigidity increased through time [*Stockmal et al.*, 1986; *Watts*, 1992; *Stewart and Watts*, 1997]. We assume a maximum value of flexural rigidity of 5.0×10^{24} Nm based on *Lyon-Caen and Molnar* [1983, 1985] and *Bilham et al.* [2003], and we adopt a minimum value of 1.0×10^{23} Nm based on values known from transitional continental lithosphere along rifted continental margins [e.g., *Stewart and Watts*, 1997; *Watts*, 2001; *Rowley*, 1998]. The thrust belt load is approximated by a rectangular block that grows from a topographic height of 2 km and a width of 50 km, to 3 km high and 250 km wide. Density of the mantle is assumed to be 3300 kg/m^3; densities of the load and the sedimentary fill in the foredeep depozone are listed on Figure 12. The foredeep was filled to approximately sea level from Eocene time onward, based on sedimentological evidence that deep-marine sedimentation ended during the late Paleocene [e.g., *Ding et al.*, 2005; *Zhu et al.*, 2005; this study]. An important source of uncertainty in this analysis is the value chosen for flexural rigidity, because this parameter exerts the first-order control on the wavelength of the flexural profile. The range of flexural rigidities used in Figure 12 is consistent with values used in previous, geophysically constrained flexural analyses of the Himalayan foreland region [*Karner and Watts*, 1983; *Lyon-Caen and Molnar*, 1985; *Duroy et al.*, 1989; *Bilham et al.*, 2003]. A second source of significant uncertainty is the amount of shortening in the thrust belt. It is also possible that the thrust belt load varied irregularly through time; we have neither evidence to suggest this nor any means by which to constrain such variations.

Constraints on the position of the flexural wave relative to the palinspastically restored thrust belt can be derived from the record of foreland basin depozones as follows (Figures 11 and 12).

1. At Sangdanlin we place the base of the foredeep at 60–58 Ma and a coeval forebulge depozone at Zhepure Mountain [*Hu et al.*, 2012; *Zhang et al.*, 2012].

2. At Zhepure Mountain, foredeep deposition began no later than ~52 Ma [*Zhu et al.*, 2005; *Najman et al.*, 2010; *Hu et al.*, 2012].
3. The Lesser Himalaya lay in a back-bulge depozone during the middle Eocene (circa 45–40 Ma), straddled the forebulge during the Oligocene [*DeCelles et al.*, 2004; *Najman et al.*, 2005; *Jain et al.*, 2009], and began to receive foredeep deposits during latest Oligocene-early Miocene time [*DeCelles et al.*, 1998a; *Najman and Garzanti*, 2000].
4. The frontal Subhimalayan zone lay within the foredeep depozone no later than ~15 Ma [*DeCelles et al.*, 1998b; *Ojha et al.*, 2009].
5. Finally, the present-day flexural profile is reasonably well known based on studies by *Lyon-Caen and Molnar* [1983, 1985] and *Bilham et al.* [2003].

The objective here is to assess whether or not the Paleogene sections presently distributed across the Himalaya could reasonably have developed along a coherent flexural profile during initial India-Asia collision and early growth of the Himalayan thrust belt. The results of the flexural model suggest that, for this to be the case, the foreland flexural wave had to migrate approximately 1300–1400 km through the region now occupied by the Himalayan thrust belt to the present Gangetic foreland basin since ~60 Ma. This distance of migration is consistent with at least 850 km of shortening, 250 km of thrust belt propagation, and approximately 250 km of increase in the wavelength of the flexural wave through time owing to increased flexural rigidity (Figure 12). It is noteworthy that the history of flexural wave migration that emerges from this model, particularly the late Paleocene through early Eocene transition from passive margin to forebulge to foredeep deposition just south of the suture zone, was recognized by *Garzanti et al.* [1987] more than 25 years ago in the northwestern (Zanskar) Himalaya.

9. Discussion

9.1. Paleogeographic Setting of the Sangdanlin Section: Oceanic Versus Continental

A key issue for interpreting the data from the Sangdanlin section is whether these strata were deposited upon oceanic or continental lithosphere. If the Sangdanlin section was deposited on oceanic lithosphere, this would indicate significant separation from Indian continental lithosphere, and the Sangdanlin section would predate collision. Evidence in support of continental, or perhaps transitional, lithosphere beneath the Sangdanlin section consists of the lithofacies of Tethyan sequence strata beneath the section, as well as the Denggang (Zhongzuo) Formation. Tethyan Jurassic and Cretaceous strata beneath the section are composed of relatively shallow marine marl, shale, sandstone, and limestone; oceanic deposits are absent. Equivalent strata in the Zhepure Mountain region consist of mixed carbonate and fine-grained clastic lithofacies deposited in hemipelagic and outer shelf to slope settings, in water no deeper than 400 m [*Willems et al.*, 1996; *Hu et al.*, 2012]. Denggang (Zhongzuo) Formation turbidites are pebbly to very coarse-grained sandstone, suggesting a short distance of transport from the nearby Indian cratonic margin, and deposition along or at the base of the north facing continental slope (Figure 10a). The only lithofacies in the Sangdanlin section that are reasonable candidates for oceanic deposits are the radiolarian chert and siliceous shale of the Sangdanlin Formation, which could have accumulated on the flexural forebulge or in the trench (Figure 10a) as the underlying Indian transitional/continental lithosphere entered the subduction zone. These observations support the interpretation that the Sangdanlin record resulted from initial collision of Indian and Asian continental lithosphere [*Ding et al.*, 2005; *Wang et al.*, 2011; *Wu et al.*, 2014].

9.2. Implications for Himalayan Shortening and the Greater India Basin

The reconstruction presented in Figure 12 is challenged by plate circuit reconstructions that suggest up to ~3600 km of post-52 Ma convergence between the Indian and Asian plates, without a comparable amount of crustal shortening in the two plates (*Molnar and Stock* [2009]; see *van Hinsbergen et al.* [2012] for a review). Recent reconstructions demonstrate that shortening or lateral extrusion in Asia cannot account for the roughly 2300–2400 km deficit in crustal shortening [*van Hinsbergen et al.*, 2011a], leading to the hypothesis that significant, to-date unrecognized, plate convergence took place within the Himalayan thrust belt during middle Cenozoic time [*van Hinsbergen et al.*, 2012]. This problem is well known from paleomagnetic and plate circuit studies of the Himalayan-Tibetan region [e.g., *Molnar and Tapponnier*, 1975; *Patriat and Achache*, 1984; *Besse et al.*, 1984; *Dewey et al.*, 1989; *Klootwijk et al.*, 1992; *Patzelt et al.*, 1996; *Molnar and Stock*, 2009; *Copley et al.*, 2010; *van Hinsbergen et al.*, 2012; *Lippert et al.*, 2014].

van Hinsbergen et al. [2012] and *Lippert et al.* [2014] also documented through paleomagnetism a 2675 ± 699 km increase in the latitudinal distance between cratonic India and the rocks of the Tethyan Himalaya that occurred between ~120 and 65 Ma. This they attributed to an extensional tectonic event that separated the rocks of the Tethyan Himalaya from the rest of India via the opening of the "Greater India basin" (GIB). As discussed by *van Hinsbergen et al.* [2012], the GIB was >1900 km wide. Geological evidence for regional extension of the Tethyan Himalaya during Early Cretaceous time consists of alkaline volcanic rocks and volcaniclastic strata exposed in a broad belt of the Tethyan Himalaya from northern India to southeastern Tibet [e.g., *Gradstein et al.*, 1991; *Garzanti and Pagni Frette*, 1991; *Gibling et al.*, 1994; *Dürr and Gibling*, 1994; *Jadoul et al.*, 1998; *Garzanti*, 1999; *Chen et al.*, 2007; *Zhu et al.*, 2009; *Hu et al.*, 2010]. Subsequent closure of the GIB was inferred to take place along the Main Central thrust in the Himalayan thrust belt. This model also requires that the Himalayan orogenic belt formed as a result of two collisions: the first during early Eocene time, between the Tethyan Himalayan block and southern Asia, and the second during latest Oligocene-early Miocene time between the Lesser Himalaya and the Greater Himalaya. Significantly, the GIB model as presented places the high-grade metamorphic rocks of the Greater Himalayan sequence above the subduction zone megathrust prior to the second collision event and thus places collision between cratonic India and the northern half of the Himalayan thrust belt at the time of activation of the Main Central thrust during the early Miocene. Although the *van Hinsbergen et al.* [2012] model involves more than simply the opening of the GIB, we will refer to it as the GIB model for the sake of brevity in the following discussion.

As presented by *van Hinsbergen et al.* [2012], the GIB model argues against any possibility that a contiguous foreland basin system could have connected cratonic India (i.e., the Lesser Himalaya) with the Tethyan Himalaya and IYS during Eocene time, because the GIB itself would have intervened between the Tethyan plus Greater Himalayan portions of the thrust belt on the upper plate and cratonic India on the lower plate. We suggest that some modifications of the GIB model would indeed make it consistent with the available geological data from the foreland basin system, as well as other geological data sets that are available from the Himalayan thrust belt.

1. The only evidence in the geological record for Cretaceous extension in the Himalaya is restricted to locations north of the South Tibetan detachment (STD) [e.g., *Hu et al.*, 2010], an early Miocene normal fault that separates the Greater Himalayan zone (on the south) from the Tethyan Himalayan zone (to the north). The logical region in which to concentrate extension during the Cretaceous would therefore be the Tethyan Himalaya. This would place the Greater Himalayan zone on the south side of the GIB, rather than on its north side as suggested by *van Hinsbergen et al.* [2012]. The early Cretaceous rocks of the southern Tethyan Himalaya [*Garzanti and Pagni Frette*, 1991; *Garzanti*, 1999] were part of a northward facing rifted margin, possibly associated with the rocks of the early Cretaceous Wölong Formation in the middle to southern Tethyan Himalaya [*Hu et al.*, 2010]. Extension related to the GIB could have reached into what is now the Lesser Himalaya, but alkali basalts and volcaniclastic strata there are probably more closely related to the Rajmahal-Sylhet eruptive events [*Sakai*, 1983, 1984] associated with passage of northeastern India over the Kerguelen hotspot [*Kent et al.*, 2002; *Coffin et al.*, 2002; *Ghatak and Basu*, 2013].
2. The GIB model as presented calls for collision between the Tethyan Himalayan block and Asia at circa 55 Ma. The data discussed in this paper from the Sangdanlin and Zhepure Mountain regions suggest that initial collision was probably several million years earlier, but in any case the age of collision reported by *van Hinsbergen et al.* [2012] is consistent with the early stages of the flexural model shown in Figure 12.
3. The foreland basin record of the Lesser Himalaya requires that detritus derived from the Tethyan Himalayan thrust belt was capable of reaching the Indian foreland region no later than about 45 Ma [*DeCelles et al.*, 1998a, 2004; *Najman et al.*, 2005; *Jain et al.*, 2009; *Ravikant et al.*, 2011]. No other source of the detrital zircon signature found in the middle Eocene rocks of the frontal Himalaya is available, and detrital zircon fission track ages demonstrate rapid exhumation in the source terrane during the Eocene. Moreover, independent evidence for shortening and uplift of Tethyan rocks during Eocene time has been reported by *Ratschbacher et al.* [1994], *Wiesmayr and Grasemann* [2002], *Murphy and Yin* [2003], *Ding et al.* [2005], *Aikman et al.* [2008], *Pullen et al.* [2011], and *Zhang et al.* [2012]. Deep tectonic burial, high-grade metamorphism, and anatexis of the Greater Himalayan sequence beneath a growing Tethyan thrust belt load during Eocene-Oligocene time is also well-documented [e.g., *Vannay and Hodges*, 1996; *Hodges et al.*, 1996; *Coleman*, 1998; *Coleman and Hodges*, 1998; *Godin et al.*, 2001; *Vannay et al.*, 2004; *Martin et al.*, 2005, 2007; *de Sigoyer et al.*, 2000; *Guillot et al.*, 2003; *Leech et al.*, 2005; *Corrie and Kohn*, 2011]. Thus, crustal

shortening and rapid exhumation in the Tethyan Himalaya, tectonic burial of Greater Himalayan rocks, and earliest foreland basin development on the Indian craton occurred coevally during Eocene-Oligocene time and provide a "hard link" between the Tethyan Himalaya and the northern Indian craton at that time. Although *van Hinsbergen et al.* [2012] argued that India was >1500 km south of the Tethyan Himalaya during the middle Eocene, their reconstruction shows a minimum separation of only ~900–500 km between 48.6 and 42.4 Ma, which is consistent with the flexural model that places the Lesser Himalayan zone in a back-bulge depozone during middle Eocene time (Figure 12). This would require that the GIB, which would have been located in what is now the southern half of the Tethyan Himalaya, must have completely closed between ~55 Ma and 45 Ma. At the rates of convergence operating during this time frame (80–150 mm/yr) [*Molnar and Stock*, 2009; *Copley et al.*, 2010], an 800–1500 km wide GIB could have been consumed in time to juxtapose the northern Indian foreland region with the Tethyan thrust belt by 45 Ma. Approximately 45 Ma closure of the GIB would also help to explain the dramatic deceleration of plate convergence rate between 50 and 45 Ma [e.g., *Molnar and Stock*, 2009; *Copley et al.*, 2010; *van Hinsbergen et al.*, 2011b].

4. The collision history advocated by *van Hinsbergen et al.* [2012] calls for closure of the GIB and collision between cratonic India and the Greater Himalayan thrust front no earlier than 25–20 Ma. This is problematic for several reasons discussed under the previous point. Most significantly, because this interpretation places the subduction zone megathrust beneath Greater Himalayan rocks, it provides no mechanism for deep burial and metamorphism of the latter. Moreover, as indicated by numerous studies of middle Eocene through Pliocene foreland basin deposits of the Lesser Himalaya and Subhimalaya, a regionally integrated foreland flexure with wavelength on the order of 1000 km, filling with shallow marine to nonmarine sediments, was migrating through the region now represented by the southern flank of the Himalayan thrust belt throughout this time interval. No evidence has been recognized in the stratigraphic records of the Lesser and Subhimalayan zones for an oceanic GIB. A modified version of the GIB model that is compatible with the tectonic history of the Greater Himalaya and the foreland basin history of the Lesser to Subhimalayan zones places the closure of the GIB at circa 45 Ma, in the region mainly north of the present outcrop distribution of the Greater Himalayan rocks (i.e., north of the South Tibetan detachment).

9.3. Remaining Uncertainties

Uncertainty remains in the nature of the link between the southern Himalayan and northern Tethyan (Zhepure Mountain) stratigraphic records of collision. In terms of sediment provenance, hard links exist between the Lesser Himalayan record and the Tethyan thrust belt, and between the Zhepure Mountain and Sangdanlin stratigraphic records and the south flank of Asia. However, the parts of the Lesser Himalayan and Zhepure Mountain records that contain detritus of northerly provenance do not overlap in time, so it remains conceivable that a large spatial gap, represented perhaps by the GIB, could have existed between cratonic India and the southern fringe of the Zhepure Mountain depositional system. The time gap, highlighted by the dashed horizontal line in Figure 12, is between the youngest part of the Zhepure Mountain section (circa 50 Ma) and the oldest Lesser Himalayan record (circa 45–40 Ma). This 5–10 Myr time gap is when the GIB, if it existed, must have closed, because the Lesser Himalayan record (Bhainskati Formation) contains detritus that ties northern cratonic India to the Tethyan thrust belt during the middle Eocene, and the Tethyan thrust belt must have incorporated the Zhepure Mountain stratigraphic section as it began to develop during the Eocene.

The flexural analysis depends on existing estimates of Himalayan shortening, which are highly uncertain. For example, displacements on most of the major thrust faults are not constrained by offsets of preserved footwall and hanging wall cutoffs; this means that Himalayan shortening is grossly underestimated. The reported amounts of shortening in the Tethyan Himalaya are anomalously low, given the rapid rates of plate convergence during late Paleocene-early Eocene time [*DeCelles et al.*, 2002]. Documentation of greater shortening in the Himalaya would help to alleviate the large discrepancy between overall crustal shortening in India and Asia, on the one hand, and plate convergence, on the other [*van Hinsbergen et al.*, 2012]. Additional work is needed to determine the amount of shortening within the Tethyan Himalaya, the nature of the basal contact of the Sangdanlin section, and geological evidence for the GIB as well as its location and timing of closure.

10. Conclusions

Results of this analysis support previous findings by *Ding et al.* [2005], *Wang et al.* [2011], and *Wu et al.* [2014] and demonstrate that sedimentary rocks at the Sangdanlin locality in the Indus-Yarlung suture zone of

southern Tibet contain the oldest documented record of the transition from Indian to Asian sediment provenance. This stratigraphic section sits atop the northern Tethyan Himalayan sequence, which was deposited on the outboard margin of Indian continental lithosphere. Detrital zircon geochronology and sedimentary petrology show that Maastrichtian-early Paleocene coarse-grained, quartz-arenitic turbidites at the base of the section were derived from rocks that now constitute the Tethyan Himalaya, and overlying feldspatholithic turbidites of Paleocene age were derived from the Gangdese arc/forearc region. Detrital zircon geochronology and a new tuff age show that this transition took place between ~60 and 58.5 Ma. We take this to be the earliest age of contact between Asia and continental lithosphere of India, and the effective age of intercontinental collision in the central part of the Himalayan orogenic belt.

Flexural modeling demonstrates that the Cenozoic strata in the Indus-Yarlung suture zone, the Tethyan Himalaya, the Lesser Himalaya, and the Subhimalaya could have been deposited within a coherent flexural wave that migrated ~1300 km across the northern flank of the late Paleocene through latest Miocene Indian continental landmass to its present location in the Gangetic foreland. This model is constrained by detrital geochronology, thermochronology, sedimentary petrology, and sedimentological data sets. Alternatively, the same data discussed herein may be compatible with a recently published model proposing that the northern part of Greater India experienced a significant extensional event—producing the Greater India basin—during the early Cretaceous. However, the Greater India basin must have closed prior to middle Eocene time in order to place the foreland region of northern cratonic India within a reasonable distance to receive detritus from the developing Tethyan Himalayan thrust belt.

Acknowledgments

Funding for this research was provided by the U.S. National Science Foundation (EAR-1008527), the Chinese Academy of Sciences (XDB03010400), and the Chinese Ministry of Science and Technology (2011CB403101). We thank Devon Orme, Peter Lippert, and Douwe van Hinsbergen for informative and animated discussions, as well as informal manuscript reviews. We are grateful to Yani Najman, Sean Long, and Tectonics Editor Nathan Niemi for reviews that helped us to improve the manuscript.

References

Aikman, A. B., T. M. Harrison, and L. Ding (2008), Evidence for early (>44 Ma) Himalayan crustal thickening, Tethyan Himalaya, southeastern Tibet, *Earth Planet. Sci. Lett.*, *274*, 14–23.

Aitchison, J. C., J. R. Ali, and A. M. Davis (2007), When and where did India and Asia collide?, *J. Geophys. Res.*, *112*, B05423, doi:10.1029/2006JB004706.

Allégre, C. J., et al. (1984), Structure and evolution of the Himalaya-Tibet orogenic belt, *Nature*, *307*, 17–22.

Besse, J., V. Courtillot, J. P. Pozzi, M. Westphal, and Y. X. Zhou (1984), Paleomagnetic estimates of crustal shortening in the Himalayan thrusts and Zangbo suture, *Nature*, *311*, 621–626, doi:10.1038/311621a0.

Bickle, M. J., H. J. Chapman, J. Bunbury, N. B. W. Harris, I. J. Fairchild, T. Ahmad, and C. Pomés (2005), Relative contributions of silicate and carbonate rocks to riverine Sr fluxes in the headwaters of the Ganges, *Geochim. Cosmochim. Acta*, *69*, 2221–2240, doi:10.1016/j.gca.2004.11.019.

Bilham, R., R. Bendick, and K. Wallace (2003), Flexure of the Indian plate and intraplate earthquakes, *Proc. Indian Acad. Sci. (Earth and Planet. Sci.)*, *112*, 1–14.

Bouma, A. H. (1962), *Sedimentology of Some Flysch Deposits: A Graphic Approach to Facies Interpretation*, 168 pp., Elsevier, Amsterdam.

Burbank, D. W., R. A. Beck, and T. Mulder (1996), The Himalayan foreland basin, in *The Tectonics of Asia*, edited by A. Yin and T. M. Harrison, pp. 205–226, Cambridge Univ. Press, New York.

Burg, J. P., and G. Chen (1984), Tectonics and structure zonation of southern Tibet, China, *Nature*, *311*, 219–223.

Burg, J. P., A. Leyreloup, J. Girardeau, and G. Chen (1987), Structure and metamorphism of a tectonically thickened continental crust: The Yalu Tsangpo suture (Tibet), *Philos. Trans. R. Soc. London, Ser. A*, *321*, 67–86.

Cai, F., L. Ding, and Y. Yue (2011), Provenance analysis of Upper Cretaceous strata in the Tethys Himalaya, southern Tibet: Implications for timing of India-Asia collision, *Earth Planet. Sci. Lett.*, *305*, 195–206.

Cai, F., L. Ding, R. J. Leary, H. Wang, Q. Xu, L. Zhang, and Y. Yue (2012), Tectonostratigraphy and provenance of an accretionary complex within the Yarlung–Zangpo suture zone, southern Tibet: Insights into subduction–accretion processes in the Neo-Tethys, *Tectonophysics*, *574–575*, 181–192.

Chen, L., X. Hu, and Z. Huang (2007), Constrains from Early Cretaceous volcaniclastic sandstones in southern Tibet on a volcanic event in the northern margin of the Indian Continent [in Chinese with English abstract], *Dizhi Xuebao*, *81*, 501–510.

Chung, S.-L., M.-F. Chu, Y. Zhang, Y. Xie, C.-H. Lo, T.-Y. Lee, C.-Y. Lan, X.-H. Li, Q. Zhang, and Y. Wang (2005), Tibetan tectonic evolution inferred from spatial and temporal variations in post-collisional magmatism, *Earth Sci. Rev.*, *68*, 173–196.

Chung, S.-L., M.-F. Chu, J. Ji, S. Y. O'Reilly, N. J. Pearson, D. Liu, T.-Y. Lee, and C.-H. Lo (2009), The nature and timing of crustal thickening in the southern Tibet: Geochemical and zircon Hf isotopic constraints from postcollisional adakites, *Tectonophysics*, *477*, 36–48.

Clift, P. D. (2006), Controls on the erosion of Cenozoic Asia and the flux of clastic sediment to the ocean, *Earth Planet. Sci. Lett.*, *241*, 571–580, doi:10.1016/j.epsl.2005.11.028.

Clift, P. D., A. Carter, and T. N. Jonell (2013), U-Pb dating of detrital zircon grains in the Paleocene Stumpata Formation, Tethyan Himalaya, Zanskar, India, *J. Asian Earth Sci.*, *82*, 80–89, doi:10.1016/j.jseaes.2013.12.014.

Coffin, M. F., M. S. Pringle, R. A. Duncan, T. P. Gladczenko, M. Storey, R. D. Müller, and L. A. Gahagan (2002), Kerguelen, hotspot magma output since 130 Ma, *J. Petrol.*, *43*, 1121–1139.

Coleman, M. E. (1998), U–Pb constraints on Oligocene–Miocene deformation and anatexis within the central Himalaya, Marsyandi valley, Nepal, *Am. J. Sci.*, *298*, 553–571.

Coleman, M. E., and K. V. Hodges (1998), Contrasting Oligocene and Miocene thermal histories from the hanging wall and footwall of the South Tibetan detachment in the central Himalaya from $^{40}Ar/^{39}Ar$ thermochronology, Marsyandi Valley, central Nepal, *Tectonics*, *17*, 726–740, doi:10.1029/98TC02777.

Copeland, P., T. M. Harrison, Y. Pan, W. S. F. Kidd, M. Roden, and Y. Zhang (1995), Thermal evolution of the Gangdese batholith, southern Tibet: A history of episodic unroofing, *Tectonics*, *14*, 223–236, doi:10.1029/94TC01676.

Copley, A., J.-P. Avouac, and J.-Y. Royer (2010), India-Asia collision and the Cenozoic slowdown of the Indian plate: Implications for the forces driving plate motions, *J. Geophys. Res.*, *115*, B03410, doi:10.1029/2009JB006634.

Corrie, S. L., and M. J. Kohn (2011), Metamorphic history of the central Himalaya, Annapurna region, Nepal, and implications for tectonic models, *Geol. Soc. Am. Bull.*, *123*, 1863–1879.
Coulon, C., H. Maluski, C. Bollinger, and S. Wang (1986), Mesozoic and Cenozoic volcanic rocks from central and southern Tibet: ^{39}Ar-^{40}Ar dating, petrological characteristics and geodynamical significance, *Earth Planet. Sci. Lett.*, *79*, 281–302.
Critelli, S., and E. Garzanti (1994), Provenance of the lower Tertiary Murree redbeds (Hazara-Kashmir Syntaxis, Pakistan) and initial rising of the Himalayas, *Sediment. Geol.*, *89*, 265–284.
Debon, F., P. LeFort, S. M. Sheppard, and J. Sonet (1986), The four plutonic belts of the Transhimalaya–Himalaya: A chemical, mineralogical, isotopic, and chronological synthesis along a Tibet–Nepal section, *J. Petrol.*, *27*, 219–250.
DeCelles, P. G. (2012), Foreland basin systems revisited: Variations in response to tectonic settings, in *Tectonics of Sedimentary Basins: Recent Advances*, edited by C. Busby and A. Pérez, pp. 405–426, John Wiley, Chichester, U. K., doi:10.1002/9781444347166.ch20.
DeCelles, P. G., G. Gehrels, J. Quade, and T. Ojha (1998a), Eocene-early Miocene foreland basin development and the history of Himalayan thrusting, western and central Nepal, *Tectonics*, *17*, 741–765, doi:10.1029/98TC02598.
DeCelles, P. G., G. E. Gehrels, J. Quade, T. P. Ojha, P. A. Kapp, and B. N. Upreti (1998b), Neogene foreland basin deposits, erosional unroofing, and the kinematic history of the Himalayan fold-thrust belt, western Nepal, *Geol. Soc. Am. Bull.*, *110*, 2–21.
DeCelles, P. G., G. E. Gehrels, J. Quade, B. Lareau, and M. Spurlin (2000), Tectonic implications of U-Pb zircon ages of the Himalayan orogenic belt in Nepal, *Science*, *288*, 497–499, doi:10.1126/science.288.5465.497.
DeCelles, P. G., D. M. Robinson, J. Quade, T. P. Ojha, C. N. Garzione, P. Copeland, and B. N. Upreti (2001), Stratigraphy, structure, and tectonic evolution of the Himalayan fold-thrust belt in western Nepal, *Tectonics*, *20*, 487–509.
DeCelles, P. G., D. M. Robinson, and G. Zandt (2002), Implications of shortening in the Himalayan fold-thrust belt for uplift of the Tibetan Plateau, *Tectonics*, *21*(6), 1062, doi:10.1029/2001TC001322.
DeCelles, P. G., G. E. Gehrels, Y. Najman, A. J. Martin, A. Carter, and E. Garzanti (2004), Detrital geochronology and geochemistry of Cretaceous–Early Miocene strata of Nepal: Implications for timing and diachroneity of initial Himalayan orogenesis, *Earth Planet. Sci. Lett.*, *227*, 313–330, doi:10.1016/j.epsl.2004.08.019.
de Sigoyer, J., V. Chavagnac, J. Blichert-Toft, I. M. Villa, B. Luais, S. Guillot, M. Cosca, and G. Mascle (2000), Dating the Indian continental subduction and collisional thickening in the northwest Himalaya: Multichronology of the Tso Morari eclogites, *Geology*, *28*, 487–490, doi:10.1130/0091-7613.
Dewey, J. F., R. M. Shackleton, C. Chengfa, and S. Yiyun (1988), The tectonic evolution of the Tibetan Plateau, *Philos. Trans. R. Soc. London, Ser. A*, *327*, 379–413.
Dewey, J. F., S. Cande, and W. C. Pitman (1989), Tectonic evolution of the India/Eurasia collision zone, *Eclog. Geol. Helv.*, *82*, 717–734.
Dickinson, W. R., and G. E. Gehrels (2009), Use of U-Pb ages of detrital zircons to infer maximum depositional ages of strata: A test against a Colorado Plateau Mesozoic database, *Earth Planet. Sci. Lett.*, *288*, 115–125, doi:10.1016/j.epsl.2009.09.013.
Dickinson, W. R., S. L. Beard, G. R. Brakenridge, J. L. Erjavec, R. C. Ferguson, K. F. Inman, R. A. Knepp, F. A. Lindberg, and P. T. Ryberg (1983), Provenance of North American Phanerozoic sandstones in relation to tectonic setting, *Geol. Soc. Am. Bull.*, *94*, 222–235.
Ding, L. (2003), Paleocene deep-water sediments and radiolarian fauna: Implications for evolution of Yarlung Zangbo foreland basin, southern Tibet, *Sci. China, Ser. D Earth Sci.*, *33*, 47–58.
Ding, L., P. Kapp, and X. Q. Wan (2005), Paleocene–Eocene record of ophiolite obduction and initial India-Asia collision, south central Tibet, *Tectonics*, *24*, TC3001, doi:10.1029/2004TC001729.
Dupont-Nivet, G., C. Hoorn, and M. Konert (2008), Tibetan uplift prior to the Eocene-Oligocene climate transition: Evidence from pollen analysis of the Xining Basin, *Geology*, *36*, 987–990, doi:10.1130/G25063A.1.
Duroy, Y., A. Farah, and R. J. Lillie (1989), Reinterpretation of the gravity field in the Himalayan foreland of Pakistan, in *Tectonics of the Western Himalayas*, *Geol. Soc. Am. Spec. Pap.*, vol. 132, edited by L. L. Malinconico and R. J. Lillie, pp. 217–236, Geological Society of America, Boulder, Colo.
Dürr, S. (1996), Provenance of Xigaze fore-arc basin clastic rocks (Cretaceous, south Tibet), *Geol. Soc. Am. Bull.*, *108*, 669–684.
Dürr, S. B., and M. R. Gibling (1994), Early Cretaceous volcaniclastic and quartzose sandstones from north central Nepal: Composition, sedimentology and geotectonic significance, *Geol. Rundsch.*, *83*, 62–75.
Einsele, G., et al. (1994), The Xigaze forearc basin: Evolution and facies architecture (Cretaceous, Tibet), *Sediment. Geol.*, *90*, 1–32.
Gaetani, M., and E. Garzanti (1991), Multicyclic history of the northern India continental margin (northwestern Himalaya), *Am. Assoc. Petrol. Geol. Bull.*, *75*, 1427–1446.
Garzanti, E. (1999), Stratigraphy and sedimentary history of the Nepal Tethys Himalaya passive margin, *J. Asian Earth Sci.*, *17*, 805–827.
Garzanti, E., and M. Pagni Frette (1991), The stratigraphic succession of the Thakkhola region (central Nepal)—Comparisons with the northwestern Tethys Himalaya, *Riv. Ital. Paleontol. Strat.*, *97*, 3–26.
Garzanti, E., A. Baud, and G. Mascle (1987), Sedimentary record of the northward flight of India and its collision with Eurasia (Ladakh Himalaya, India), *Geodin. Acta*, *1*, 297–312.
Gehrels, G. E., V. A. Valencia, and J. Ruiz (2008), Enhanced precision, accuracy, efficiency, and spatial resolution of U-Pb ages by laser ablation-multicollector-inductively coupled plasma-mass spectrometry, *Geochem. Geophys. Geosyst.*, *9*, Q03017, doi:10.1029/2007GC001805.
Gehrels, G. E., et al. (2011), Detrital zircon geochronology of pre-Tertiary strata in the Tibetan-Himalayan orogen, *Tectonics*, *30*, TC5016, doi:10.1029/2011TC002868.
Gervais, A., B. Savoye, T. Mulder, and E. Gonthier (2006), Sandy modern turbidite lobes: A new insight from high resolution seismic data, *Mar. Petrol. Geol.*, *23*, 485–502.
Ghatak, A., and A. R. Basu (2013), Isotopic and trace element geochemistry of alkalic–mafic–ultramafic–carbonatitic complexes and flood basalts in NE India: Origin in a heterogeneous Kerguelen plume, *Geochem. Cosmochim. Acta*, *115*, 46–72.
Gibling, M. R., F. M. Gradstein, I. L. Kiristiansen, J. Nagy, M. Sarti, and J. Wiedmann (1994), Early Cretaceous strata of the Nepal Himalayas: Conjugate margins and rift volcanism during Gondwanan breakup, *J. Geol. Soc. London*, *151*, 269–290.
Girardeau, J., J. Marcoux, and Y. Zao (1984), Lithologic and tectonic environment of the Xigaze ophiolite (Yarlung Zangbo suture zone, southern Tibet, China), and kinematics of its emplacement, *Eclog. Geol. Helv.*, *77*, 153–170.
Godin, L., R. R. Parrish, R. L. Brown, and K. V. Hodges (2001), Crustal thickening leading to exhumation of the Himalayan Metamorphic core of central Nepal: Insight from U-Pb Geochronology and ^{40}Ar/^{39}Ar Thermochronology, *Tectonics*, *20*, 729–747, doi:10.1029/2000TC001204.
Gradstein, F. M., M. R. Gibling, M. Sarti, U. von Rad, J. W. Thurow, J. G. Ogg, L. F. Jansa, M. A. Kaminski, and G. E. G. Westermann (1991), Mesozoic Tethyan strata of Thakkhola, Nepal: Evidence for the drift and breakup of Gondwana, *Palaeogeogr. Palaeoclimatol. Palaeoecol.*, *88*, 193–218.
Green, O. R., M. P. Searle, R. I. Corfield, and R. M. Corfield (2008), Cretaceous-Tertiary carbonate platform evolution and the age of the India-Asia collision along the Ladakh Himalaya (Northwest India), *J. Geol.*, *116*, 331–353.

Guillot, S., E. Garzanti, D. Baratoux, D. Marquer, G. Mahéo, and J. de Sigoyer (2003), Reconstructing the total shortening history of the NW Himalaya, *Geochem. Geophys. Geosyst.*, *4*(7), 1064, doi:10.1029/2002GC000484.

Guilmette, C., R. Hébert, C. Dupuis, C. S. Wang, and Z. J. Li (2008), Metamorphic history and geodynamic significance of high-grade metabasites from the ophiolitic mélange beneath the Yarlung Zangbo ophiolites, Xigaze area, Tibet, *J. Asian Earth Sci.*, *32*, 423–437.

Guilmette, C., R. Hébert, C. Wang, and M. Villeneuve (2009), Geochemistry and geochronology of the metamorphic sole underlying the Xigaze Ophiolite, Yarlung Zangbo Suture Zone, South Tibet, *Lithos*, *112*, 149–162.

He, S., P. Kapp, P. G. DeCelles, G. E. Gehrels, and M. Heizler (2007), Cretaceous–Tertiary geology of the Gangdese Arc in the Linzhou area, southern Tibet, *Tectonophysics*, *433*, 15–37.

Hébert, R., R. Bezard, C. Guilmette, J. Dostal, C. S. Wang, and Z. F. Liu (2011), The Indus–Yarlung Zangbo ophiolites from Nanga Parbat to Namche Barwa syntaxes, southern Tibet: First synthesis of petrology, geochemistry and geochronology with incidences on geodynamic reconstructions of Neo-Tethys, *Gondwana Res.*, *22*, 377–397.

Henderson, A. L., Y. Najman, R. Parrish, M. BouDagher-Fadel, D. Barford, E. Garzanti, and S. Andò (2010), Geology of the Cenozoic Indus Basin sedimentary rocks: Paleoenvironmental interpretation of sedimentation from the western Himalaya during the early phases of India-Eurasia collision, *Tectonics*, *29*, TC6015, doi:10.1029/2009TC002651.

Hodges, K. V., R. R. Parrish, and M. P. Searle (1996), Tectonic evolution of the central Annapurna Range, Nepalese Himalayas, *Tectonics*, *15*, 1264–1291, doi:10.1029/96TC01791.

Hren, M. T., C. P. Chamberlain, G. E. Hilley, P. M. Blisniuk, and B. Bookhagen (2007), Major ion chemistry of the Yarlung Tsangpo-Brahmaputra river: Chemical weathering, erosion, and CO2 consumption in the southern Tibetan plateau and eastern syntaxis of the Himalaya, *Geochim. Cosmochim. Acta*, *71*, 2907–2935.

Hu, X., L. Jansa, L. Chen, W. L. Griffin, S. Y. O'Reilly, and J. Wang (2010), Provenance of Lower Cretaceous Wolong volcaniclastics in the Tibetan Himalaya: Implications for the final breakup of eastern Gondwana, *Sediment. Geol.*, *223*, 193–205.

Hu, X., H. D. Sinclair, J. Wang, H. Jiang, and F. Wu (2012), Late Cretaceous-Palaeogene stratigraphic and basin evolution in the Zhepure Mountain of southern Tibet: Implications for the timing of India-Asia initial collision, *Basin Res.*, *24*, 1–24.

Jadoul, F., F. Brerra, and E. Garzanti (1998), The Tethys Himalayan passive margin from Late Triassic to Early Cretaceous (South Tibet), *J. Asian Earth Sci.*, *16*, 173–194.

Jaeger, J. J., V. Courtillot, and P. Tapponnier (1989), Paleontological view of the ages of the Deccan Traps, the Cretaceous/Tertiary boundary, and the India-Asia collision, *Geology*, *17*, 316–319.

Jain, A. K., N. Lal, B. Sulemani, A. K. Awasthi, S. Singh, R. Kumar, and D. Kumar (2009), Detrital-zircon fission-track ages from the Lower Cenozoic sediments, NW Himalayan foreland basin: Clues for exhumation and denudation of the Himalaya during the India-Asia collision, *Geol. Soc. Am. Bull.*, *121*, 519–535.

Kapp, P., A. Yin, T. M. Harrison, and L. Ding (2005), Cretaceous-Tertiary shortening, basin development, and volcanism in central Tibet, *Geol. Soc. Am. Bull.*, *117*, 865–878, doi:10.1130/B25595.1.

Karner, G. D., and A. B. Watts (1983), Gravity anomalies and flexure of the lithosphere at mountain ranges, *J. Geophys. Res.*, *88*(B12), 10,449–10,477, doi:10.1029/JB088iB12p10449.

Kent, R. W., M. S. Pringle, R. D. Müller, A. D. Saunders, and N. C. Ghose (2002), 40Ar/39Ar Geochronology of the Rajmahal Basalts, India, and their relationship to the Kerguelen Plateau, *J. Petrol.*, *43*, 1141–1153.

Klootwijk, C. T., J. S. Gee, J. W. Peirce, G. M. Smith, and P. L. McFadden (1992), An early India-Asia contact: Paleomagnetic constraints from Ninetyeast Ridge, ODP Leg 121, *Geology*, *20*, 395–398.

Lee, H. Y., S. L. Chung, C. H. Lo, J. Q. Ji, T. Y. Lee, Q. Qian, and Q. Zhang (2009), Eocene Neotethyan slab breakoff in southern Tibet inferred from the Linzizong volcanic record, *Tectonophysics*, *477*, 20–35.

Leech, M. L., S. Singh, A. K. Jain, S. L. Klemperer, and R. M. Manickavasagarn (2005), The onset of India–Asia continental collision: Early, steep subduction required by the timing of UHP metamorphism in the western Himalaya, *Earth Planet. Sci. Lett.*, *234*, 83–97, doi:10.1016/j.epsl.2005.02.038.

Li, Y., C. Wang, X. Hu, M. Bak, J. Wang, and L. Chen (2007), Characteristics of Early Eocene radiolarian assemblages of the Saga area, southern Tibet and their constraint on the closure history of the Tethys, *Chin. Sci. Bull.*, *52*, 2108–2114.

Lippert, P. C., D. J. J. van Hinsbergen, and G. Dupont-Nivet (2014), The Early Cretaceous to present latitude of the central Lhasa-plano (Tibet): A paleomagnetic synthesis with implications for Cenozoic tectonics, paleogeography, and climate of Asia, in *Towards an Improved Understanding of Uplift Mechanisms and the Elevation History of the Tibetan Plateau*, *Geol. Soc. Am. Spec. Pap.*, edited by J. S. Nie, G. D. Hoke, and B. K. Horton, pp. 1–21, Geol. Soc. of Am., Boulder, Colo.

Long, S., N. McQuarrie, T. Tobgay, and D. Grujic (2011), Geometry and crustal shortening of the Himalayan fold-thrust belt, eastern and central Bhutan, *Geol. Soc. Am. Bull.*, *123*, 1427–1447, doi:10.1130/B30203.1.

Lowe, D. R. (1982), Sediment gravity flows: II. Depositional models with special reference to deposits of high-density turbidity currents, *J. Sediment. Petrol.*, *52*, 279–297.

Lowe, D. R., and R. D. LoPiccolo (1974), The characteristics and origins of dish and pillar structures, *J. Sediment. Petrol.*, *44*, 484–501.

Lyon-Caen, H., and P. Molnar (1983), Constraints on the structure of the Himalaya from an analysis of gravity anomalies and a flexural model of the lithosphere, *J. Geophys. Res.*, *88*, 8171–8191, doi:10.1029/JB088iB10p08171.

Lyon-Caen, H., and P. Molnar (1985), Gravity anomalies, flexure of the Indian plate, and the structure, support and evolution of the Himalaya and Ganga basin, *Tectonics*, *4*, 513–538, doi:10.1029/TC004i006p00513.

Maluski, H., F. Proust, and X. C. Xia (1982), ^{39}Ar-^{40}Ar dating of the trans-Himalayan calc-alkaline magmatism of southern Tibet, *Nature*, *298*, 152–154.

Martin, A. J., P. G. DeCelles, G. E. Gehrels, P. J. Patchett, and C. Isachsen (2005), Isotopic and structural constraints on the location of the Main Central Thrust in the Annapurna Range, central Nepal Himalaya, *Geol. Soc. Am. Bull.*, *117*, 926–944, doi:10.1130/B25646.1.

Martin, A., G. E. Gehrels, and P. G. DeCelles (2007), The tectonic significance of (U, Th)/Pb ages of monazite inclusions in garnet from the Himalaya of central Nepal, *Chem. Geol.*, *244*, 1–24, doi:10.1016/j.chemgeo.2007.05.003.

McBride, E. F. (1963), A classification of common sandstones, *J. Sediment. Res.*, *33*, 664–669.

Métivier, F. Y., P. Gaudemer, and M. K. Tapponnier (1999), Mass accumulation rates in Asia during the Cenozoic, *Geophys. J. Int.*, *137*, 280–318.

Molnar, P., and J. M. Stock (2009), Slowing of India's convergence with Eurasia since 20 Ma and its implications for Tibetan mantle dynamics, *Tectonics*, *28*, TC3001, doi:10.1029/2008TC002271.

Molnar, P., and P. Tapponnier (1975), Cenozoic tectonics of Asia: Effects of a continental collision, *Science*, *189*, 419–426.

Molnar, P., W. R. Boos, and D. S. Battisti (2010), Orographic controls on climate and paleoclimate of Asia: Thermal and mechanical roles for the Tibetan Plateau, *Annu. Rev. Earth Planet. Sci.*, *38*, 77–102.

Mulder, T., and J. Alexander (2001), The physical character of subaqueous sedimentary density flows and their deposits, *Sedimentology*, *48*, 269–299.

Murphy, M. A. (2007), Isotopic characteristics of the Gurla Mandhata metamorphic core complex: Implications for the architecture of the Himalayan orogen, *Geology*, *35*, 983–986.
Murphy, M. A., and A. Yin (2003), Structural evolution and sequence of thrusting in the Tethyan fold-thrust belt and Indus-Yalu suture zone, southwest Tibet, *Geol. Soc. Am. Bull.*, *115*, 21–34.
Mutti, E. (1992), *Turbidite Sandstones*, 275 pp., Azienda Generale Italiana Petroli, Parma, Italy.
Mutti, E., T. H. Nilsen, and F. Ricci Lucchi (1978), Outer fan depositional lobes of the Laga Formation (Upper Miocene and Lower Pliocene), east-central Italy, in *Sedimentation in Submarine Canyons, Fans, and Trenches*, edited by D. J. Stanley and G. Kelling, pp. 210–223, Dowden, Hutchinson & Ross, Stroudsburg, Pa.
Mutti, E., and W. R. Normark (1991), An integrated approach to the study of turbidite systems, in *Seismic Facies and Sedimentary Processes of Submarine Fans and Turbidite Systems*, edited by P. Weimer and M. H. Link, pp. 75–104, Springer, New York.
Mutti, E., and F. Ricci Lucchi (1975), Turbidite facies and facies associations, in *Examples of Turbidite Facies and Associations From Selected Formations of the Northern Apennines*, IX Int. Congr. Sedimentol. Field Trip A-11, pp. 21–36, Nice, Fr.
Najman, Y. (2006), The detrital record of orogenesis: A review of approaches and techniques used in the Himalayan sedimentary basins, *Earth Sci. Rev.*, *74*, 1–72.
Najman, Y., and E. Garzanti (2000), Reconstructing early Himalayan tectonic evolution and paleogeography from Tertiary foreland basin sedimentary rocks, northern India, *Geol. Soc. Am. Bull.*, *112*(3), 435–449, doi:10.1130/0016-7606(2000)112<435:REHTEA>2.0.CO;2.
Najman, Y., P. Clift, M. R. W. Johnson, and A. H. F. Robertson (1993), Early stages of foreland basin evolution in the Lesser Himalaya, N. India, in *Himalayan Tectonics*, edited by P. J. Treloar and M. P. Searle, *Geol. Soc. Spec. Publ.*, *74*, 541–558.
Najman, Y., A. Carter, G. Oliver, and E. Garzanti (2005), Provenance of Eocene foreland basin sediments, Nepal: Constraints to the timing and diachroneity of early Himalayan orogenesis, *Geology*, *33*, 309–312, doi:10.1130/G21161.1.
Najman, Y., et al. (2008), The Paleogene record of Himalayan erosion: Bengal Basin, Bangladesh, *Earth Planet. Sci. Lett.*, *273*, 1–14, doi:10.1016/j.epsl.2008.04.028.
Najman, Y., et al. (2010), Timing of India-Asia collision: Geological biostratigraphic, and paleomagnetic constraints, *J. Geophys. Res. 115*, B12416, doi:10.1029/2010JB007673.
Normark, W. R. (1978), Fan valleys, channels, and depositional lobes on modern submarine fans: Characters for recognition of sandy turbidites environments, *Am. Assoc. Pet. Geol. Bull.*, *62*, 912–931.
Ojha, T. P., R. F. Butler, P. G. DeCelles, and J. Quade (2009), Magnetic polarity stratigraphy of the Neogene foreland basin deposits of Nepal, *Basin Res.*, *21*, 61–90.
Orme, D. A., B. Carrapa, and P. Kapp (2014), Sedimentology, provenance and geochronology of the Upper Cretaceous-Lower Eocene western Xigaze forearc, southern Tibet, *Basin Res.*, in press.
Patriat, P., and J. Achache (1984), India-Eurasia collision chronology has implications for crustal shortening and driving mechanism of plates, *Nature*, *311*, 615–620.
Patzelt, A., H. Li, J. Wang, and E. Appel (1996), Palaeomagnetism of Cretaceous to Tertiary sediments from southern Tibet: Evidence for the extent of the northern margin of India prior to the collision with Eurasia, *Tectonophysics*, *259*, 259–284, doi:10.1016/0040-1951(95)00181-6.
Pivnik, D. A., and N. A. Wells (1996), The transition from Tethys to the Himalaya as recorded in northwest Pakistan, *Geol. Soc. Am. Bull.*, *108*, 1295–1313.
Pullen, A., P. Kapp, P. G. DeCelles, G. E. Gehrels, and L. Ding (2011), Cenozoic anatexis and exhumation of Tethyan Sequence rocks in the Xiao Gurla Range, southwest Tibet, *Tectonophysics*, *501*, 28–40.
Quade, J., N. English, and P. G. DeCelles (2003), Silicate versus carbonate weathering in the Himalaya: A comparison of the Arun and Seti River watersheds, *Chem. Geol.*, *202*, 275–296.
Ratschbacher, L., W. Frisch, G. Liu, and C. Chen (1994), Distributed deformation in southern and western Tibet during and after the India–Asia collision, *J. Geophys. Res.*, *99*, 19,917–19,945, doi:10.1029/94JB00932.
Ravikant, V., F.-Y. Wu, and W.-Q. Ji (2011), U–Pb age and Hf isotopic constraints of detrital zircons from the Himalayan foreland Subathu sub-basin on the Tertiary palaeogeography of the Himalaya, *Earth Planet. Sci. Lett.*, *304*, 356–368.
Ravizza, G. E., and J. C. Zachos (2003), Records of Cenozoic ocean chemistry, in *Treatise on Geochemistry*, *Oceans Mar. Geochem.*, vol. 6, edited by H. D. Holland and K. K. Turekian, pp. 551–581, Pergamon, Oxford, U. K., doi:10.1016/B0-08-043751-6/06121-1.
Robinson, D. M., P. G. DeCelles, and P. Copeland (2006), Tectonic evolution of the Himalayan thrust belt in western Nepal: Implications for channel flow models, *Geol. Soc. Am. Bull.*, *118*, 865–885.
Rowley, D. B. (1996), Age of initiation of collision between India and Asia: A review of stratigraphic data, *Earth Planet. Sci. Lett.*, *145*, 1–13.
Rowley, D. B. (1998), Minimum age of initiation of collision between India and Asia north of Everest based on the subsidence history of the Zhepure Mountain section, *J. Geol.*, *106*, 229–235.
Sakai, H. (1983), Geology of the Tansen Group of the Lesser Himalaya in Nepal, *Mem. Fac. Sci. Kyushu Univ. Ser. D*, *25*, 27–74.
Sakai, H. (1984), Stratigraphy of Tansen area in the Nepal Lesser Himalayas, *J. Nepal Geol. Soc.*, *4*, 41–52.
Schärer, U., R. H. Xu, and C. J. Allégre (1984), U-Pb geochronology of Gangdese (Transhimalaya) plutonism in the Lhasa-Xigaze region, Tibet, *Earth Planet. Sci. Lett.*, *69*, 311–320.
Searle, M. P., et al. (1987), The closing of Tethys and the tectonics of the Himalaya, *Geol. Soc. Am. Bull.*, *98*, 678–701.
Singh, S., M. M. Sarin, and C. France-Lanord (2005), Chemical erosion in the eastern Himalaya: Major ion composition of the Brahmaputra and d13C of dissolved inorganic carbon, *Geochim. Cosmochim. Acta*, *69*, 3573–3588.
Stewart, J., and A. B. Watts (1997), Gravity anomalies and spatial variations of flexural rigidity at mountain ranges, *J. Geophys. Res.*, *102*, 5327–5352, doi:10.1029/96JB03664.
Stockmal, G., C. Beaumont, and R. Boutilier (1986), Geodynamic models of convergent margin tectonics: Transition from rifted margin to overthrust belt and consequences for foreland basin development, *Am. Assoc. Pet. Geol. Bull.*, *70*, 181–190.
Talling, P. J., D. G. Masson, E. J. Sumner, and G. Malgesini (2012), Subaqueous sediment density flows: Depositional processes and deposit types, *Sedimentology*, *59*, 1937–2003.
Turcotte, D. L., and G. Schubert (2006), *Geodynamics: Applications of Continuum Physics to Geological Problems*, 456 pp., John Wiley, New York.
van Hinsbergen, D. J. J., P. Kapp, G. Dupont-Nivet, P. G. DeCelles, P. C. Lippert, and T. H. Torsvik (2011a), Restoration of Cenozoic deformation of Asia, and the size of Greater India, *Tectonics*, *30*, TC5003, doi:10.1029/2011TC002908.
van Hinsbergen, D. J. J., B. Steinberger, P. V. Doubrovine, and R. Gassmoller (2011b), Acceleration and deceleration of India-Asia convergence since the Cretaceous: Roles of mantle plumes and continental collision, *J. Geophys. Res.*, *116*, B06101, doi:10.1029/2010JB008051.
van Hinsbergen, D. J. J., P. C. Lippert, G. Dupont-Nivet, N. McQuarrie, P. V. Doubrovine, W. Spakman, and T. H. Torsvik (2012), Greater India Basin hypothesis and a two-stage Cenozoic collision between India and Asia, *Proc. Natl. Acad. Sci. U.S.A.*, *109*, 7659–7664.

Vannay, J.-C., and K. V. Hodges (1996), Tectonometamorphic evolution of the Himalayan metamorphic core between the Annapurna and Dhaulagiri, central Nepal, *J. Metamorph. Geol.*, *14*, 635–656.
Vannay, J.-C., B. Grasemann, M. Rahn, W. Frank, A. Carter, V. Baudraz, and M. Cosca (2004), Miocene to Holocene exhumation of metamorphic crustal wedges in the NW Himalaya: Evidence for tectonic extrusion coupled to fluvial erosion, *Tectonics*, *23*, TC1014, doi:10.1029/2002TC001429.
Walker, R. G. (1975), Generalized facies models for resedimented conglomerates of turbidite association, *Geol. Soc. Am. Bull.*, *86*, 737–748.
Walker, R. G. (1985), Mudstones and thin-bedded turbidites associated with the Upper Cretaceous Wheeler Gorge Conglomerates, California: A possible channel-levee complex, *J. Sediment. Petrol.*, *55*, 279–290.
Walton, E. K. (1967), The sequence of internal structures in turbidites, *Scott. J. Geol.*, *3*, 306–317.
Wang, C., X. Li, Z. Liu, Y. Li, L. Jansa, J. Dai, and Y. Wei (2012), Revision of the Cretaceous–Paleogene stratigraphic framework, facies architecture and provenance of the Xigaze forearc basin along the Yarlung Zangbo suture zone, *Gondwana Res.*, *22*, 415–433.
Wang, C. S., X. H. Li, X. M. Hu, and L. F. Jansa (2002), Latest marine horizon north of Qomolangma (Mt Everest): Implications for closure of Tethys seaway and collision tectonics, *Terra Nova*, *14*, 114–120.
Wang, J., X. Hu, L. Jansa, and Z. Huang (2011), Provenance of the Upper Cretaceous–Eocene deep-water sandstones in Sangdanlin, southern Tibet: Constraints on the timing of initial India-Asia Collision, *J. Geol.*, *119*, 293–309.
Watts, A. B. (1992), The effective elastic thickness of the lithosphere and the evolution of foreland basins, *Basin Res.*, *4*, 169–178.
Watts, A. B. (2001), *Isostasy and Flexure of the Lithosphere*, 478 pp., Cambridge Univ. Press, Cambridge.
Weimer, P. (1989), Sequence stratigraphy of the Mississippi Fan (Plio-Pleistocene), Gulf of Mexico, *Geo-Mar. Lett.*, *9*, 185–272.
Wiesmayr, G., and B. Grasemann (2002), Eohimalayan fold and thrust belt: Implications for the geodynamic evolution of the NW-Himalaya (India), *Tectonics*, *21*(6), 1058, doi:10.1029/2002TC001363.
Willems, H., Z. Zhou, B. Zhang, and K.-U. Grafe (1996), Stratigraphy of the Upper Cretaceous and Lower Tertiary strata in the Tethyan Himalayas of Tibet (Tingri area, China), *Geol. Rundsch.*, *85*, 723–754.
Wu, F.-Y., W. Q. Ji, J.-G. Wang, C.-Z. Liu, S.-L. Chung, and P. D. Clift (2014), Zircon U-Pb and Hf isotopic constraints on the onset time of India-Asia collision, *Am. J. Sci.*, *314*, 548–579.
Xu, R. H., U. Schärer, and C. J. Allégre (1985), Magmatism and metamorphism in the Lhasa block (Tibet): A geochronological study, *J. Geol.*, *93*, 41–57, doi:10.1086/628918.
Yang, Z., F. Bi, W. Zhang, Y. Zhang, and Z. Zhang (2003), Geological map of Saga region, 1:250,000, Geological Publishing House, Beijing.
Yin, A. (2006), Cenozoic tectonic evolution of the Himalayan orogen as constrained by along-strike variation of structural geometry, exhumation history, and foreland sedimentation, *Earth Sci. Rev.*, *76*, 1–131.
Yin, A., and T. M. Harrison (2000), Geologic evolution of the Himalayan-Tibetan Orogen, *Annu. Rev. Earth Planet. Sci.*, *28*, 211–280.
Zhang, Q., H. Willems, L. Ding, K.-U. Gräfe, and E. Appel (2012), Initial India-Asia Continental collision and foreland basin evolution in the Tethyan Himalaya of Tibet: Evidence from stratigraphy and paleontology, *J. Geol.*, *120*, 175–189.
Zhu, B., W. S. F. Kidd, D. B. Rowley, B. S. Currie, and N. Shafique (2005), Age of initiation of the India-Asia collision in the east-central Himalaya, *J. Geol.*, *113*, 265–285.
Zhu, D.-C., S.-L. Chung, X.-X. Mo, Z.-D. Zhao, Y. Niu, B. Song, and Y. H. Yang (2009), The 132 Ma Comei-Bunbury large igneous province: Remnants identified in present-day southeastern Tibet and southwestern Australia, *Geology*, *37*, 583–586.